

Electronic density of states of a $U(1)$ quantum spin liquid with spinon Fermi surface. I. Orbital magnetic field effects

Wen-Yu He^{1,*} and Patrick A. Lee^{2,†}

¹*School of Physical Science and Technology, ShanghaiTech University, Shanghai 201210, China*

²*Department of Physics, Massachusetts Institute of Technology, Cambridge, Massachusetts 02139, USA*



(Received 1 February 2023; revised 10 May 2023; accepted 15 May 2023; published 31 May 2023)

A quantum spin liquid with a spinon Fermi surface is an exotic insulator that hosts neutral Fermi surfaces inside the insulating gap. In an external magnetic field, it has been pointed out that the neutral Fermi surfaces are Landau quantized to form Landau levels due to the coupling to the induced emergent gauge magnetic field. In this paper, we calculate the electronic density of states (as observed in tunneling experiments) of the quantum spin liquid in an orbital magnetic field. We find that the Landau levels from the neutral Fermi surfaces give rise to a set of steps emerging at the upper and lower Hubbard band edges. Each of the Hubbard band edge steps further develop into a band edge resonance peak when a weak gauge binding arising from the gauge field fluctuations is taken into account. Importantly, each Hubbard band edge step and its resulting resonance peak in the weak gauge binding are found to have a corresponding Landau level from the neutral Fermi surfaces, so the Hubbard band edge steps and the band edge resonance peaks provide signatures to the unique feature that characterizes the Landau quantization of the in-gap neutral Fermi surfaces in the spin liquid. We further consider the strong gauge-binding regime where the band edge resonance peaks move into the Mott gap and develop into true in-gap bound states. In the strong gauge binding regime, we solve the Landau-level spectrum of the in-gap bound states in an orbital magnetic field. For the in-gap bound state with a Mexican-hat-like band dispersion, we find that the envelop energy to have a state excited from the bound state Landau levels decreases quadratically with the magnetic field. The quadratic decrease behavior of the envelop energy is consistent with the intuition that applying magnetic field localizes the states and energetically promotes the in-gap bound states formation. Finally, we discuss the connection of our results to the electronic density of states spectra measured in the layered 1T-TaS₂. We point out that a quantum spin liquid with a quasibound state in the upper Hubbard band can give the density of states spectra similar to the one measured in the experiment.

DOI: [10.1103/PhysRevB.107.195155](https://doi.org/10.1103/PhysRevB.107.195155)

I. INTRODUCTION

Quantum spin liquid (QSL), due to its close connections to the high-temperature superconductivity phenomenon [1,2] and potential applications in topological quantum computations [3,4], has been a long-sought state of matter since Anderson's first proposal in 1973 [5]. As a QSL is an exotic insulator with no traditional Landau order parameter down to zero temperature [2,6,7], the search for QSL states in real materials becomes extremely difficult. Among various types of QSLs, the gapless $U(1)$ QSL with a spinon Fermi surface (SFS) is featured by charge neutral spin excitations living on the neutral Fermi surfaces [2,8,9], so its experimental identification focuses on detecting the neutral Fermi surfaces inside the insulating gap.

One seminal idea to detect the neutral Fermi surfaces in the gapless $U(1)$ QSL is built on the effect of Landau quantization [10,11]. In a $U(1)$ QSL with SFS, an electron is fractionalized into a spinon and a chargon. The spinon is a charge-neutral fermion that carries spin $1/2$, while the chargon is a charged boson that carries the electric charge. The spinon and the

chargon are coupled through an emergent $U(1)$ gauge field [8]. In the presence of an external orbital magnetic field B , an emergent gauge magnetic field (EGMF) b is induced on the spinons and the remaining magnetic field on the chargons is $B - b$ [8,10,11]. Since the induced EGMF on the spinons Landau quantizes the neutral Fermi surfaces in the $U(1)$ QSL, the $U(1)$ QSL was predicted to have quantum oscillations (QOs) of resistivity and magnetization in spite of its insulating nature [10,11]. However, up to now, this effect has not been seen experimentally.

QOs in the insulating states of matter are highly unusual as the canonical understanding of QOs is based on the existence of electronic Fermi surfaces [12]. Recently, a few experimental observations of QOs in insulators were reported [13–17], and Landau quantization of the neutral Fermi surfaces inside the insulating gap was suggested to be one possible origin of the observed QOs. However, Landau quantization of the neutral Fermi surfaces is sufficient for QOs in an insulator but not necessary. It has been known that a band insulator with a hybridization gap can also have QOs that arise from the gap size modulation by magnetic field [18–21]. Therefore, extrinsic effects need to be ruled out before one can conclude that the observations necessarily indicate the Landau quantization of the in-gap neutral Fermi surfaces. To detect the neutral Fermi surfaces in a $U(1)$ QSL by the effect of Landau quantization,

*hewy@shanghaitech.edu.cn

†palee@mit.edu

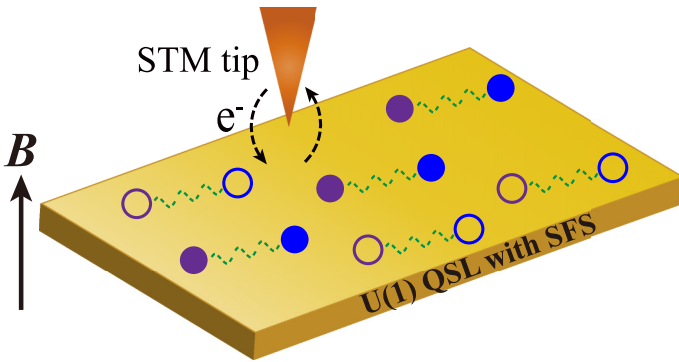


FIG. 1. The STM setup to measure the local electronic DOS in the QSL. An electron injected into the QSL is fractionalized into a spinon and a chargon. The filled blue and purple circles denote the spinons and doublons, respectively. The empty blue and purple ones represent the spinon holes and holons, respectively. Wavy lines indicate the spinon chargon attraction due to the $U(1)$ gauge field fluctuations.

it will be desirable to find evidence of the Landau quantization of the neutral Fermi surfaces other than QOs.

One possibility is to directly observe the effect of Landau levels by tunneling spectroscopy. For a band insulator in an orbital magnetic field, the electronic density of states (DOS) is known to be a set of discrete Delta-function-like peaks that originate from the electronic Landau levels (LLs) in each band. For a $U(1)$ QSL with a SFS, since the QSL electron is a composite particle composed of a chargon and a spinon, its electronic DOS in an orbital magnetic field requires a comprehensive consideration of the chargon DOS and the spinon DOS along with the magnetic field partition between them. So far, the nature of the electronic DOS of a $U(1)$ QSL with SFS in an orbital magnetic field and how it compares to that of a band insulator has not been studied in any detail. This is the main goal of this paper.

The electron spectral function and the local DOS for a Mott insulator with a SFS has been studied in Ref. [22] in zero magnetic field. At the mean-field level, the electronic spectrum for a given momentum \mathbf{k} (as measured by angle-resolved photo-emission spectroscopy) is given by the convolution of the spinon and chargon spectra in frequency and momentum. For the upper and lower Hubbard bands (UHB, LHB), the minimum excitation involves a gapped chargon with energy Δ and a gapless spinon at the spinon Fermi momentum \mathbf{k}_F . Therefore, the excitations have an energy threshold at Δ which occurs in a ring in momentum space with radius given by the Fermi momentum \mathbf{k}_F . A continuum of excitation appears above the threshold and the spectral function goes as $\sqrt{E - \Delta}$ above the gap. The local DOS is obtained by integrating over momentum space. A common way to measure the local DOS is by scanning tunneling microscopy (STM) as shown in Fig. 1. The STM tip injects an electron or hole into the system, and breaks up into spinon and chargon. The local DOS was found to increase linearly with energy above the threshold [22].

Beyond mean field, one has to consider the effect of gauge field fluctuations. In Refs. [22–24], the dominant effect is considered via the screened longitudinal gauge field fluctuations

which they model with a short range attraction U_b . This is illustrated in Fig. 1. Beyond a certain interaction strength, a bound state was found to split off from edge of the Hubbard band. In this paper, we explore in greater detail the intermediate coupling strength regime and find that a resonance is formed near the band edge.

Recently, several STM measurements have been carried out to detect the possible QSL phases on the surface of bulk 1T-TaS₂ [25–28], monolayer 1T-TaSe₂ [29–31], and 1T/1H-TaS₂ heterostructures [32]. These data show clear upper and LHBs as rather broad peaks in the DOS spectra with a rather sharp onset. Interestingly, the data on monolayer 1T-TaS₂ grown on oriented graphite [32] shows rather linear onsets in both the UHB and LHB, in agreement with the prediction of Ref. [22]. Furthermore, on the surface of the layered 1T-TaS₂, an extra resonance peak with sidebands was found near the UHB edge [27]. In a subsequent measurement, an external magnetic field is applied [33], and the UHB edge resonance peak was found to move towards the Mott gap center as the magnetic field increases as B^2 . These data motivate us to examine the local DOS in greater detail, first without a magnetic field and then with an orbital magnetic field. Even in zero B field, the spectrum is far from being free-electron-like. Therefore, we expect more complicated behavior than the naive expectation that the continuum of states will be replaced by a set of discrete LLs.

For a $U(1)$ QSL in an orbital magnetic field B , a physical electron is composed of a spinon in the spinon LLs and a chargon in the chargon LLs, where the spinon LLs and chargon LLs are induced by the EGMF b and the remaining magnetic field $B - b$, respectively. The magnetic field partition between the spinons and the chargons is determined by the Ioffe-Larkin rule [34,35]. For a gapless $U(1)$ QSL that occurs in the weak Mott regime [36–39], the Ioffe-Larkin rule indicates that the EGMF b dominates over the remaining magnetic field $B - b$. Since the spinon LL spacing is much larger than that of the chargons, each time a spinon LL is filled will cause a sudden increase in the electronic DOS. Near the energies of Hubbard band edges, such sudden changes of electronic DOS are manifested as a few steps, and those steps have one-to-one correspondence to the spinon LLs. Since the orbital magnetic field induced band-edge steps in the QSL electronic DOS are in sharp contrast to the discrete Delta function like peaks in that of a band insulator, those steps represent a unique feature of a gapless $U(1)$ QSL in an orbital magnetic field.

Next we consider the effect of spinon-chargon binding. We find that when the gauge binding is weak, with no external magnetic field, the electronic DOS develop a pair of resonance peaks at the bottom of the UHB and the top of the LHB. As the binding interaction increases, the pair of band edge resonance peaks gradually moves inside the Mott gap and eventually develops into a pair of in-gap bound states.

In the presence of an orbital magnetic field, it is found that for weak gauge binding each band edge step in the QSL electronic DOS at zero U_b evolves into a resonance peak, which is the precursor of binding between a spinon in the spinon LLs and a chargon. Inherited from the band edge steps at zero U_b , each band edge resonance peak is intrinsically connected to a LL from the neutral Fermi surfaces as well. For the QSL with a weak gauge binding, the external magnetic field

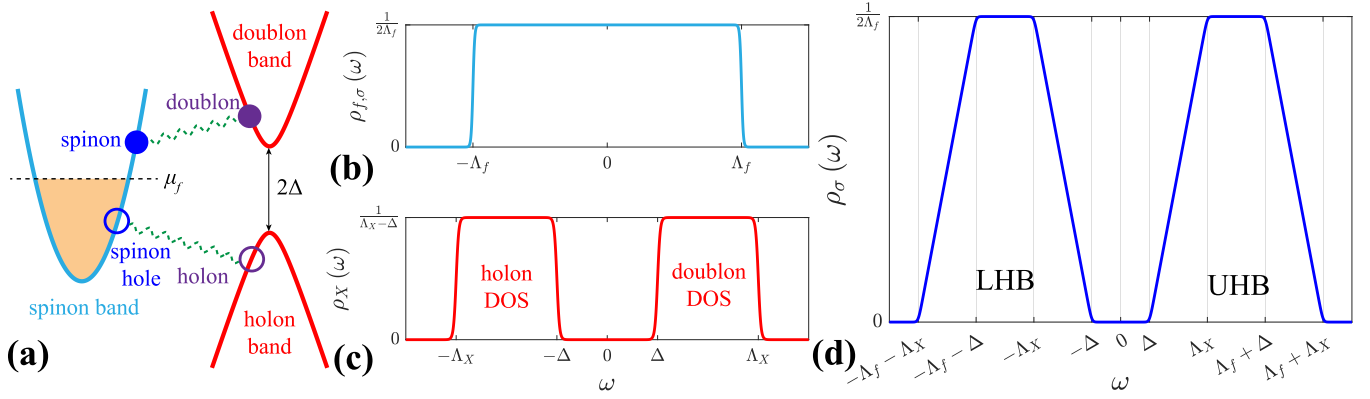


FIG. 2. Electron fractionalization in a $U(1)$ QSL with SFS and the resulting electronic DOS, calculated in mean-field theory without accounting for gauge field fluctuations. In the QSL, an electronic excitation is composed of a spinon excitation and a doublon, while a hole state is composed of a spinon hole and a holon. Holons and doublons are the chargons that carry charge $\pm e$, respectively. In the case of $B = 0T$ in (a), the spinons, holons, and doublons all live in the quadratic bands. The spinons are coupled to the chargons through an emergent $U(1)$ gauge field that is denoted by the green wavy lines. The quadratic band dispersions in (a) give rise to the constant DOS of the spinons in (b) and that of the chargons in (c). After convolution, the resulting QSL electronic DOS $\rho_\sigma(\omega)$ in $B = 0T$ is given in (d). The orange shaded region in (a) represents the spinon Fermi sea filled by the spinons. Here Δ denotes the Mott insulating gap and ω denotes the energy.

induced Landau quantization of the neutral Fermi surfaces is thus characterized by the set of band edge resonance peaks emerging in the QSL electronic DOS.

Next we consider the case of strong gauge binding. With increasing gauge binding, the resonance peaks begin to move into the Mott gap. In a magnetic field, these discrete in-gap peaks in a sufficiently large gauge binding correspond to the LLs of the in-gap bound states. By solving the binding equation of spinon LL states and chargons, we obtain the bound state LL spectrum. For the in-gap bound state with a Mexican-hat-like band dispersion, we find that the envelop energy to have a state excited from the bound state LL spectrum decreases quadratically with B . The quadratic decrease of the envelop energy with B matches the intuition that the energy saved in the binding increases as the spinons get more localized in the magnetic field.

The goal of this paper is to calculate the electronic DOS of a $U(1)$ with SFS in an orbital magnetic field. In the first stage, the spinon and chargon are treated as noninteracting. In the second stage, the gauge binding from the $U(1)$ gauge field fluctuations is taken into account to see how the electronic DOS gets affected. In the study, the regimes of zero gauge binding, weak gauge binding, and strong gauge binding are all covered so the orbital magnetic field effects on the electronic DOS of a $U(1)$ QSL with SFS are comprehensively understood. The rest of the paper is organized as follows. In Sec. II, the fractionalization of an electron into a spinon and a chargon is introduced for a $U(1)$ QSL with SFS. In a two-dimensional system, given the spinon DOS and the chargon DOS, the electronic DOS of the gapless $U(1)$ QSL at $B = 0T$ is obtained. In Sec. III, the gapless $U(1)$ QSL in an orbital magnetic field is shown to have the Landau quantization that gives rise to steps at the Hubbard band edges. Those band edge steps in the QSL electronic DOS are found to have intrinsic connections to the spinon LLs. In Sec. IV, by numerically calculating the electronic DOS of a gapless $U(1)$ QSL in a triangular lattice, we confirm that the orbital magnetic field induced spinon Landau quantization gives rise to the band

edge steps that emerge in the QSL electronic DOS. In Sec. V, the gauge binding U_b from the $U(1)$ gauge field fluctuations is added to the QSL. The QSL electronic DOS at $B = 0T$ is obtained in both the weak and strong gauge binding regime. The evolution of the QSL electronic DOS with the increase of U_b is given. In Sec. VI, the orbital magnetic field effects on the QSL electronic DOS are considered in both the weak and strong gauge binding regime. In Sec. VII, we deal with the QSL in the strong gauge binding regime. The bound state band dispersions are analyzed in the continuum model at $B = 0T$. In a finite magnetic field, the binding equations for the in-gap bound states are derived and the bound state LL spectrum is numerically solved. In Sec. VIII, we connect our results of the QSL electronic DOS in an orbital magnetic field to the electronic DOS spectra measured by STM in the layered 1T-TaS₂ [33]. In Sec. IX, we give a brief conclusion to our results.

II. ELECTRON FRACTIONALIZATION IN A QSL AND THE LOCAL ELECTRONIC DOS

In a $U(1)$ QSL with SFS, electrons go through the spin-charge separation and are fractionalized into spinons and chargons. In the slave rotor formalism, the mean-field Hamiltonian for the $U(1)$ QSL with SFS takes the form [40,41]

$$H_0 = \sum_k \epsilon_k (a_{-k} a_{-k}^\dagger + b_k^\dagger b_k) + \sum_{k,\sigma} \xi_k f_{\sigma,k}^\dagger f_{\sigma,k}, \quad (1)$$

with $a_{-k}^{(\dagger)}$, $b_k^{(\dagger)}$, and $f_{\sigma,k}^{(\dagger)}$ being the annihilation (creation) operators for a holon, doublon, and spinon, respectively. Here $\sigma = \uparrow/\downarrow$ denotes the spin index. The holons and doublons are the nonrelativistic approximation to the relativistic chargons near the Hubbard band edges [8]. A holon carries the charge $+e$ as that in a hole excitation, while a doublon carries the charge $-e$ as that in an electron. For the spinons, the spinon band ξ_k has the spinon chemical potential μ_f lying inside the band, so there exist neutral Fermi surfaces that bring about the gapless spin excitations, as indicated in Fig. 2(a). For the

holons and doublons, the energy spectrum $\epsilon_{\mathbf{k}}$ are gapped so there exists a gap for charge excitations as shown in Fig. 2(a). In the assumption of deconfinement [42,43], the $U(1)$ QSL with SFS is a charge insulator but exhibits metallic behavior in the spin channel.

In the $U(1)$ QSL, due to the fractionalization, a physical electron is composed of a spinon and a chargon. In the QSL, to create an electronic state requires creating a spinon and a doublon together or creating a spinon and simultaneously annihilating a holon. The operator to create an electron is written as $c_{\mathbf{k},\mathbf{k}',\sigma}^\dagger = f_{\sigma,\mathbf{k}}^\dagger (a_{-\mathbf{k}'} + b_{\mathbf{k}'}^\dagger)$, so the Matsubara Green's function for an electronic state in the QSL is constructed from the convolution [22,41]

$$G_\sigma(i\omega_n, \mathbf{k}, \mathbf{k}') = -\frac{1}{\beta} \sum_{\nu_n} G_{f,\sigma}(i\omega_n - i\nu_n, \mathbf{k}) \times [G_a(-i\nu_n, -\mathbf{k}') + G_b(i\nu_n, \mathbf{k}')], \quad (2)$$

with $\beta = (k_b T)^{-1}$ being the thermodynamic beta, $\omega_n = (2n + 1)\pi\beta^{-1}$ and $\nu_n = 2n\pi\beta^{-1}$ being the fermionic and bosonic Matsubara frequencies, respectively. Here $G_{f,\sigma}(i\omega_n, \mathbf{k}) = (i\omega_n - \xi_{\mathbf{k}})^{-1}$ is the spinon Matsubara Green's function, $G_a(-i\nu_n, -\mathbf{k}) = (-i\nu_n - \epsilon_{\mathbf{k}})^{-1}$ is the holon Matsubara Green's function, and $G_b(i\nu_n, \mathbf{k}) = (i\nu_n - \epsilon_{\mathbf{k}})^{-1}$ is the doublon Matsubara Green's function. After summing over the Matsubara frequencies, one can perform the analytic continuation $i\omega_n \rightarrow \omega + i0^+$ to get the retarded electronic Green's function,

$$G_\sigma^R(\omega, \mathbf{k}, \mathbf{k}') = \frac{n_F(\xi_{\mathbf{k}}) + n_B(\epsilon_{\mathbf{k}'})}{\omega + i0^+ - \xi_{\mathbf{k}} + \epsilon_{\mathbf{k}'}} + \frac{n_F(-\xi_{\mathbf{k}}) + n_B(\epsilon_{\mathbf{k}'})}{\omega + i0^+ - \xi_{\mathbf{k}} - \epsilon_{\mathbf{k}'}} \quad (3)$$

with $n_F(\xi) = \frac{1}{2}(1 - \tanh \frac{\beta\xi}{2})$ and $n_B(\epsilon) = \frac{1}{2}(\coth \frac{\beta\epsilon}{2} - 1)$ being the Fermi distribution function and Bose distribution function, respectively. In this section, we discuss the local DOS as measured by an STM experiment. For a QSL with translational symmetry, the local electronic DOS counts all the allowed \mathbf{k} and \mathbf{k}' modes, so the number of electronic states per energy per unit cell is [41]

$$\rho_\sigma(\omega) = \frac{1}{N^2} \sum_{\mathbf{k},\mathbf{k}'} n_F(\xi_{\mathbf{k}}) \delta(\omega - \xi_{\mathbf{k}} + \epsilon_{\mathbf{k}'}) + \frac{1}{N^2} \sum_{\mathbf{k},\mathbf{k}'} n_F(-\xi_{\mathbf{k}}) \delta(\omega - \xi_{\mathbf{k}} - \epsilon_{\mathbf{k}'}), \quad (4)$$

with N being the number of lattice sites. From here, we refer the number of states per energy per unit cell to the DOS. In Eq. (4), the Bose factor has been dropped in the low-temperature regime $k_b T \ll \min[\epsilon_{\mathbf{k}}] = \Delta$. Here Δ denotes the Mott gap.

The QSL electronic DOS obtained in Eq. (4) provides a clear picture of how the compositions of the spinons and the chargons contribute to the total electronic DOS. In the $U(1)$ QSL with SFS, a spinon hole inside the spinon Fermi sea together with a holon forms a hole state, while a spinon excitation above the spinon Fermi level combined with a doublon gives rise to an electronic excitation, as illustrated in Fig. 2(a). Since the combination of a spinon state with a quasimomentum \mathbf{k} and a chargon state with a quasimomentum

\mathbf{k}' is arbitrary, the total number of the combinations gives the number of states in the QSL. The first term in Eq. (4) counts the number of hole states, so it gives the DOS in the LHB. Similarly, the second term in Eq. (4) counts the number of electronic excitations, so it gives the DOS in the UHB.

By applying Eq. (4), one can obtain the electronic DOS of a two-dimensional $U(1)$ QSL with SFS. The spinon band and the chargon band in the QSL can be approximated by the quadratic dispersions: $\xi_{\mathbf{k}} = \frac{\hbar^2 \mathbf{k}^2}{2m_f} - \mu_f$ and $\epsilon_{\mathbf{k}} = \frac{\hbar^2 \mathbf{k}^2}{2m_x} + \Delta$, respectively. In the quadratic band approximation, as long as the energy lies inside the bands, the DOS always takes the constant value. The spinon DOS takes $\rho_{f,\sigma}(\omega) = \frac{m_f A_c}{2\pi \hbar^2}$ for $\omega \in [-\Lambda_f, \Lambda_f]$, as plotted in Fig. 2(b). For the chargons, the holons in the range $\omega \in [-\Lambda_x - \Delta, -\Delta]$ and the doublons in the range $\omega \in [\Delta, \Lambda_x + \Delta]$ both contribute to the constant DOS $\rho_x(\omega) = \frac{m_x A_c}{2\pi \hbar^2}$ as plotted in Fig. 2(c). Here A_c is the unit cell area, $\Lambda_f = \frac{\pi \hbar^2}{m_f A_c}$ and $\Lambda_x = \frac{2\pi \hbar^2}{m_x A_c} + \Delta$ are the energy cut-offs introduced for the bands of the spinons and the chargons, respectively. Both the spinon DOS and the chargon DOS show an abrupt increase from zero at the band edges. Given the spinon DOS and the chargon DOS, the QSL electronic DOS is then evaluated and plotted in Fig. 2(d). One can observe that the electronic DOS shows finite slopes at the Hubbard band edges [22], which is consistent with Eq. (4) that the number of states increases linearly from zero as the energy crosses from $|\omega| = \Delta$ into the bulk Hubbard bands. Here the simple quadratic approximation for the spinon and chargon band dispersions has been adopted, but one can see in Sec. IV below that the quadratic band approximation captures all the key features present in the more realistic QSL electronic DOS calculated in a lattice model.

III. LANDAU QUANTIZATION AND THE ELECTRONIC DOS OF A QSL

An orbital magnetic field B applied to a $U(1)$ QSL is divided into two parts: an EGMF b on the spinons and a remaining magnetic field $B - b$ on the chargons [8–10]. The spinons and the chargons are both Landau quantized as schematically shown in Fig. 3(a), so the mean field Hamiltonian in Eq. (1) now becomes

$$H_0(b, B - b) = \sum_{n,m} \epsilon_n (a_{n,m} a_{n,m}^\dagger + b_{n,m}^\dagger b_{n,m}) + \sum_{n,m,\sigma} \xi_n f_{n,m,\sigma}^\dagger f_{n,m,\sigma}. \quad (5)$$

Here ϵ_n are the chargon LLs induced by $B - b$, and ξ_n represent the spinon LLs arising from the EGMF b . The operators $a_{n,m}^\dagger$, $b_{n,m}^\dagger$, and $f_{n,m}^\dagger$ are the annihilation (creation) operator for a holon, doublon, and spinon in the n th LL, respectively. The index m counts the LL degeneracy.

As the orbital magnetic field B introduces Landau quantization, an electronic state in the $U(1)$ QSL is now composed of a spinon LL state and a chargon LL state. The creation operator of an electronic state now takes the form $c_{n,m,n',m',\sigma}^\dagger = f_{n,m,\sigma}^\dagger (a_{n',m'} + b_{n',m'}^\dagger)$. Similar to the case of $B = 0$ T, the electronic Matsubara Green's function in an orbital magnetic field

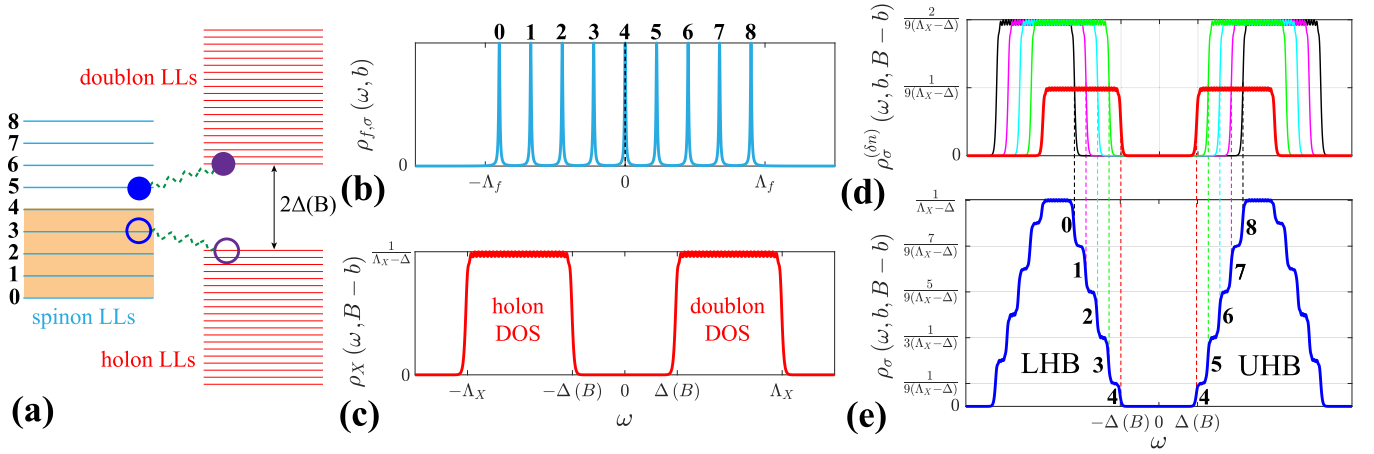


FIG. 3. Landau quantizations in the QSL and DOS. This figure is designed to be compared with Figs. 2(a)–2(d), which describe the case of zero magnetic field. In a finite orbital magnetic field B , the bands of the spinons and chargons are Landau quantized to form the LLs in (a). For the QSL that occurs in the weak Mott regime, the spinon LL spacing $\hbar\omega_f$ is larger than the chargon LL spacing $\hbar\omega_X$. In the temperature region $\hbar\omega_X < k_b T \ll \hbar\omega_f$, the spinon LLs give rise to a set of Dirac Delta function like peaks in the spinon DOS $\rho_{f,\sigma}(\omega, b)$ in (b), while the chargon LLs are thermally broadened, generating the chargon DOS $\rho_X(\omega, B-b)$ in (c) with a few ripples representing the chargon LLs. In (b), the black dashed line denotes the spinon chemical potential $\mu_f(b)$, and the $n=4$ spinon LL is assumed to be half filled. In this case, a hole state in the LHB is composed of a spinon hole in the $n=4, 3, 2, 1, 0$ LLs and a holon. An electronic excitation in the UHB is composed of a spinon excitation in the $n=4, 5, 6, 7, 8$ LLs and a doublon. The resulting electronic DOS is $\rho_\sigma(\omega, b, B-b) = \sum_{\delta n=0}^4 \rho_\sigma^{(\delta n)}(\omega, b, B-b)$, which includes five terms. The DOS $\rho_\sigma^{(\delta n)}(\omega, b, B-b)$ with $\delta n = 0, 1, 2, 3, 4$ correspond to the red, green, cyan, magenta, and black lines, respectively, in (d). Summing over all the spinon LL index as indicated in Eq. (9) gives the total electronic DOS $\rho_\sigma(\omega, b, B-b)$ in (e), which shows a few steps near the Hubbard band edges. The Hubbard band edge steps in (e) originate from the abrupt change of $\rho_\sigma^{(\delta n)}(\omega, b, B-b)$ in (d) as demonstrated by the dashed lines in (d) and (e). Each Hubbard band edge step is labeled by one spinon LL index. The orange shaded region in (a) means that the spinon LL states there are occupied.

B is constructed from the convolution [41],

$$G_{n,m,n',m',\sigma}(i\omega_n) = -\frac{1}{\beta} \sum_{\nu_n} G_{f,n,m,\sigma}(i\omega_n - i\nu_n) \times [G_{a,n',m'}(-i\nu_n) + G_{b,n',m'}(i\nu_n)], \quad (6)$$

with $G_{f,n,m,\sigma}(i\omega_n) = (i\omega_n - \xi_n)^{-1}$, $G_{a,n,m}(-i\nu_n) = (-i\nu_n - \epsilon_n)^{-1}$, and $G_{b,n,m}(i\nu_n) = (i\nu_n - \epsilon_n)^{-1}$ being the Matsubara Green's function of the spinon, holon, and doublon LL states, respectively. After performing the Matsubara frequency summation, one gets the retarded Green's function for the QSL electronic state:

$$G_{n,m,n',m',\sigma}^R(\omega) = \frac{n_F(\xi_n) + n_B(\epsilon_{n'})}{\omega + i0^+ - \xi_n + \epsilon_{n'}} + \frac{n_F(-\xi_n) + n_B(\epsilon_{n'})}{\omega + i0^+ - \xi_n - \epsilon_{n'}}. \quad (7)$$

For the QSL in an orbital magnetic field B , as the number of electronic states counts all the states in the LLs, the electronic DOS takes the form

$$\rho_\sigma(\omega, b, B-b) = \frac{1}{N^2} \sum_{n,m,n',m'} n_F(\xi_n) \delta(\omega - \xi_n + \epsilon_{n'}) + \frac{1}{N^2} \sum_{n,m,n',m'} n_F(-\xi_n) \delta(\omega - \xi_n - \epsilon_{n'}). \quad (8)$$

Here the Bose factor has been dropped in the low-temperature regime as is done in the case of $B=0$ T.

Comparing Eqs. (8) and (4), one finds that the electronic DOS in a finite B has a similar form to the electronic DOS at

$B=0$ T, except that the quasimomentum in Eq. (4) is replaced by the LL index in Eq. (8). The two terms in Eq. (8) have a similar physical meaning as those in Eq. (4). In an orbital magnetic field B , both the spinon bands and the chargon bands are Landau quantized to form LLs as schematically shown in Fig. 3(a). For the $U(1)$ QSL in a magnetic field, a hole state is composed of a spinon hole from a filled (or partial filled) spinon LL and a holon LL state. The number of hole states equals to the total combinations of the occupied spinon LL states and the hole LL states, which is captured by the first term in Eq. (8). Similarly, a spinon excitation in an empty (or partial filled) spinon LL combined with a doublon LL state gives rise to an electronic excitation in the QSL. The number of electronic excitations is the total combination of the unoccupied spinon LL states and the doublon LL states, which uncorresponds to the second term in Eq. (8). Therefore, the LHB DOS and the UHB DOS in a finite orbital magnetic field are given by the first and second terms in Eq. (8), respectively.

To obtain the QSL electronic DOS from Eq. (8), one needs to know the magnetic field partition between the spinons and the chargons. It is known from the Ioffe-Larkin rule [34,35] that the EGMF b takes $b = \alpha B = \chi_X B / (\chi_X + \chi_f)$, with χ_f and χ_X being the diamagnetic susceptibility of the spinons and the chargons, respectively. In the temperature region where $k_b T$ is larger than the LL spacing, the diamagnetic susceptibility of the spinon is $\chi_f = \frac{e^2}{12\pi m_f}$, and that of the chargon has been calculated to be $\chi_X = \frac{e^2 v^2}{24\pi \Delta}$ [44], with v being the relativistic chargon velocity. Now the ratio α takes $\alpha = m_f v^2 / (m_f v^2 + 2\Delta)$. It is clear that the ratio α approaches 1 in the small gap limit. As the gapless $U(1)$ QSL phase tends

to occur in the weak Mott regime [36–39], it is reasonable to assume that the EGMF b on the spinons dominates over the remaining $B - b$ on the chargons. It indicates that the spinon LL spacing is much larger than the chargon LL spacing in reality.

In the quadratic band approximation, the LL spectrum of the spinon and the chargon are $\xi_n = (n + \frac{1}{2})\hbar\omega_f - \mu_f(b)$ and $\epsilon_n = (n + \frac{1}{2})\hbar\omega_X + \Delta$, respectively. Here $\omega_f = \frac{eb}{m_f}$ and $\omega_X = \frac{e(B-b)}{m_X}$ are the cyclotron frequencies of the spinon and chargon, respectively. The spinon chemical potential $\mu_f(b)$ is determined by the equation $\sum_{n=0}^{\infty} 1/n_F(\xi_n) = \nu$ with $\nu = \frac{\mu_f}{\hbar\omega_f}$ being the spinon LL filling factor [41]. Due to the spinon Landau quantization, the chemical potential $\mu_f(b)$ oscillates with b and approaches the spinon Fermi energy μ_f when $b \rightarrow 0$. The evolution of $\mu_f(b)$ with b can be found in Fig. S1 in the Supplemental Material [41]. In the temperature region $\hbar\omega_X < k_bT \ll \hbar\omega_f$, the spinon DOS $\rho_{f,\sigma}(\omega, b)$ is composed of a set of Dirac Delta function like peaks as schematically plotted in Fig. 3(b), while the chargon LL peaks are smoothed by the thermal fluctuations. As a result, the chargon DOS $\rho_X(\omega, B - b)$ in a finite magnetic field in Fig. 2(c) is almost the same as that in Fig. 3(c) with $B = 0$ T. The DOS $\rho_X(\omega, B - b)$ in Fig. 3(c) differs from that in Fig. 2(c) only in two aspects: (1) in Fig. 3(c), the thermally smoothed LL peaks appear like ripples and (2) in Fig. 3(c), the Mott gap $\Delta(B) = \Delta + \frac{1}{2}\hbar\omega_X$ increases with B . The linear increase of Mott gap with B reflects the internal distribution of B on the chargons.

In an orbital magnetic field, suppose that the QSL has its spinons filled up to the $n = n_0$ spinon LL, the electronic DOS calculated from Eq. (8) reads [41]

$$\begin{aligned} \rho_\sigma(\omega, b, B - b) &= \sum_{n=0}^{n_0} \frac{\lambda_n}{\nu} \rho_h[\omega + (n_0 - n)\hbar\omega_f, B - b] \\ &+ \sum_{n=n_0}^{n_c} \frac{1 - \lambda_n}{\nu} \rho_d[\omega - (n - n_0)\hbar\omega_f, B - b], \quad (9) \end{aligned}$$

with λ_n being the filling of the n th spinon LL and $\nu = \sum_n \lambda_n$. Here $\rho_h(\omega, B - b)$ and $\rho_d(\omega, B - b)$ denote the DOS of the holons and doublons, respectively. Please note that the summation of the holon DOS and doublon DOS gives the chargon DOS: $\rho_X(\omega, B - b) = \rho_h(\omega, B - b) + \rho_d(\omega, B - b)$, which can be inferred from Figs. 2(c) and 3(c). The n_c is introduced as a cutoff in the spinon LL because the spinon band has a finite bandwidth.

To illustrate the QSL electronic DOS in an orbital magnetic field, we consider a spinon system that has its $n = 4$ LL half filled as indicated in Fig. 3(b). The total QSL electronic DOS calculated from Eq. (9) is written as $\rho_\sigma(\omega, b, B - b) = \sum_{\delta n=0}^4 \rho_\sigma^{(\delta n)}(\omega, b, B - b)$, which includes five terms:

$$\begin{aligned} \rho_\sigma^{(\delta n)}(\omega, b, B - b) &= \begin{cases} \frac{1}{9}\rho_X(\omega, B - b), & \delta n = 0 \\ \frac{2}{9}\rho_h(\omega + \delta n\hbar\omega_f, B - b) \\ + \frac{2}{9}\rho_d(\omega - \delta n\hbar\omega_f, B - b), & \delta n \neq 0. \end{cases} \quad (10) \end{aligned}$$

Here we have set $\delta n = |n - n_0|$. The DOS $\rho_\sigma^{(\delta n)}(\omega, b, B - b)$ with $\delta n = 0, 1, 2, 3, 4$ are plotted in red, green, cyan, magenta, and black, respectively in Fig. 3(d). By performing the summation over all the spinon LL indices n , we eventually arrive at the QSL electronic DOS plotted in Fig. 3(e). Importantly, since the chargon DOS $\rho_X(\omega, B - b)$ shows an abrupt increase at the threshold energy $\omega = \pm\Delta(B)$, the QSL electronic DOS obtained by summing all the energy-shifted chargon DOS in Eq. (10) exhibits a set of steps emerging near the Hubbard band edges, as can be seen in Fig. 3(e). Here we have assumed the half filling of the $n = 4$ spinon LL, so an equal number of spinon holes and spinon excitations in the $n = 4$ LL are involved in the formation of physical electronic states. Therefore, the resulting two steps at $\omega = \pm\Delta(B)$ in Fig. 3(e) are of the same height. More generally, the height of the two steps at $\omega = \pm\Delta(B)$ differs as the filling λ_{n_0} deviates from $1/2$. Specifically, the step at $-\Delta(B)$ increases from 0 to $\frac{1}{\nu(\Lambda_X - \Delta)}$ and the step at $\Delta(B)$ accordingly decreases from $\frac{1}{\nu(\Lambda_X - \Delta)}$ to 0 as the filling λ_{n_0} increases from 0 to 1. When the applied magnetic field is so small that $\hbar\omega_f < k_bT$, those steps would be thermally smoothed and the electronic DOS consistently approaches the case of $B = 0$ T shown in Fig. 2(d). Importantly, Eq. (9) for the electronic DOS of the QSL with SFS applies to an arbitrary magnetic field partition between the spinons and chargons. In an orbital magnetic field, as long as the EGMF b on the spinons dominates over the remaining field $B - b$ on the chargons, the Hubbard band edge steps arising from the spinon LLs can always be identified in the electronic DOS spectra, given the temperature respecting $k_bT \ll \hbar\omega_f$.

IV. THE QSL ELECTRONIC DOS IN A TRIANGULAR LATTICE MODEL

To verify the two-dimensional QSL electronic DOS obtained in Secs. II and III, we consider a gapless $U(1)$ QSL in a triangular lattice and perform a more realistic calculation for the electronic DOS in the lattice model. The band dispersions for the spinon and the chargon in the triangular lattice are taken to be

$$\begin{aligned} \xi_k &= -2t_f \left(2 \cos \frac{1}{2}k_x a \cos \frac{\sqrt{3}}{2}k_y a + \cos k_x a \right) - \mu_f, \quad (11) \\ \epsilon_k &= -2t_X \left(2 \cos \frac{1}{2}k_x a \cos \frac{\sqrt{3}}{2}k_y a + \cos k_x a - 3 \right) + \Delta, \quad (12) \end{aligned}$$

where a is the lattice constant. The band-structure parameters are set to be $t_f = 0.03$ eV, $t_X = 0.02$ eV, and $\Delta = 0.25$ eV. Here the spinon chemical potential takes $\mu_f = 0.025$ eV to make the spinon band half-filled. At zero magnetic field, the spinon DOS reads

$$\rho_{f,\sigma}(\omega) = -\frac{1}{N\pi} \sum_k \text{Im} \frac{1}{\omega + i0^+ - \xi_k} \quad (13)$$

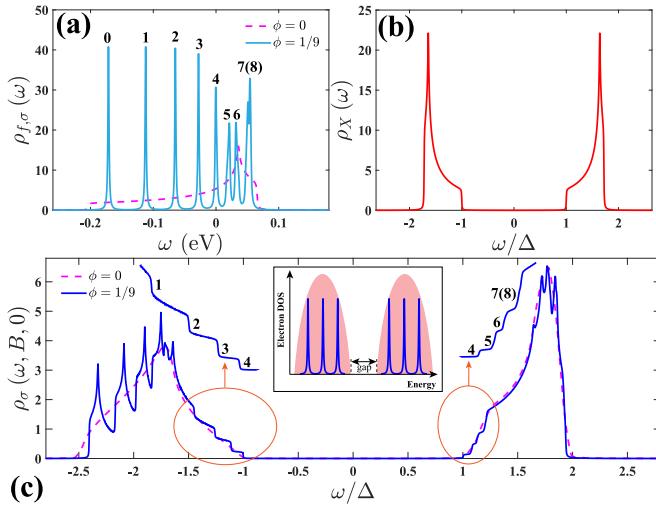


FIG. 4. (a) The DOS of the spinons in a triangular lattice. Given a magnetic flux ratio $\phi = 1/9$, the continuous spinon DOS is Landau discretized into nine peaks. (b) The chargon DOS in the triangular lattice. (c) The QSL electronic DOS calculated in the triangular lattice model. The spinon Landau quantization induces a few steps near the Hubbard band edges, giving the unique feature of the spinon Landau quantization in the QSL. The middle inset is the schematic showing the electronic DOS of a band insulator. In an orbital magnetic field B , the continuous spectrum (pink shaded regions) below and above the gap are Landau quantized into Dirac Delta function like peaks colored in blue. In the magnetic field, the QSL electronic DOS exhibits a unique feature that is completely different from the electronic DOS of a band insulator.

and is plotted as the dashed magenta line in Fig. 4(a). The chargon DOS takes

$$\rho_X(\omega) = -\frac{1}{N\pi} \sum_k \text{Im} \left(\frac{1}{\omega + i0^+ + \epsilon_k} + \frac{1}{\omega + i0^+ - \epsilon_k} \right) \quad (14)$$

and is plotted in Fig. 4(b). The spinon DOS at the band bottom in Fig. 4(a) and that of the chargon at $\omega = \pm\Delta$ in Fig. 4(b) both show an abrupt increase from zero, which agree well with the quadratic band approximation results. The QSL electronic DOS $\rho_\sigma(\omega)$ in the triangular lattice can then be obtained through Eqs. (2)–(4). In Fig. 4(c), $\rho_\sigma(\omega)$ is plotted as the magenta dashed line. At the threshold energy $\omega = \pm\Delta$, the QSL electronic DOS $\rho_\sigma(\omega)$ from the lattice model also shows the finite slope, consistent with that from the quadratic band approximation in Sec. II.

For the QSL in an orbital magnetic field B , since the magnetic field breaks the lattice translational symmetry, its mean-field Hamiltonian in Eq. (1) needs to be reconstructed as [41]

$$\hat{H}_0 = \sum_k [\hat{a}_{-k} \hat{h}_X(\mathbf{k}) \hat{a}_{-k}^\dagger + \hat{b}_k^\dagger \hat{h}_X(\mathbf{k}) \hat{b}_k] + \sum_{\sigma,k} \hat{f}_{\sigma,k}^\dagger \hat{h}_f(\mathbf{k}) \hat{f}_{\sigma,k}. \quad (15)$$

Here the annihilation (creation) operators $\hat{a}_{-k}^{(\dagger)}$, $\hat{b}_k^{(\dagger)}$ and $\hat{f}_{\sigma,k}^{(\dagger)}$ are column vectors with each element representing a state at one site in the magnetic unit cell. The matrices $\hat{h}_f(\mathbf{k})$ and

$\hat{h}_X(\mathbf{k})$ represent the mean-field tight-binding Hamiltonian for the spinons in the EGMF b and the chargons in the remaining field $B - b$, respectively. In principle, both $\hat{h}_f(\mathbf{k})$ and $\hat{h}_X(\mathbf{k})$ should be the Hofstadter Hamiltonian matrices in the triangular lattice, but it is extremely difficult to deal with the two gauge fields b and $B - b$ simultaneously in the same lattice. Since the EGMF b is supposed to be much larger than the remaining magnetic field $B - b$, we push it to the limit of $b \rightarrow B$ so in the lattice model the orbital magnetic field is only acted on the spinons.

The detail form of the spinon Hofstadter Hamiltonian matrix $\hat{h}_f(\mathbf{k})$ in a rational magnetic flux ratio $\phi = \frac{eB}{h} \frac{\sqrt{3}a^2}{2}$ is given in the Supplemental Material [41]. The chargon mean field Hamiltonian matrix $\hat{h}_X(\mathbf{k})$ in zero magnetic flux can be also found in the Supplemental Material [41]. Here $\hat{h}_X(\mathbf{k})$ is constructed in the magnetic unit cell so a chargon can be combined with a spinon in the same site to form a physical electron. Now, for the multiband system, the spinon DOS is

$$\rho_{f,\sigma}(\omega, b = B) = -\frac{1}{N\pi} \sum_k \text{trIm} \frac{1}{\omega + i0^+ - \hat{h}_f(\mathbf{k})} \quad (16)$$

and the chargon DOS $\rho_X(\omega, B - b = 0)$ takes the same value as that calculated in Eq. (14). The electronic retarded Green's function matrix elements for the multiband system are found to be [41]

$$\begin{aligned} \hat{G}_{\sigma,k,l}^R(\omega, \mathbf{k}, \mathbf{k}') &= \sum_{i,i'} \hat{U}_{f,k,i}(\mathbf{k}) \hat{U}_{X,k',i'}(\mathbf{k}') \left[\frac{n_F(\xi_{k,i}) + n_B(\epsilon_{k',i'})}{\omega + i0^+ - \xi_{k,i} + \epsilon_{k',i'}} \right. \\ &\quad \left. + \frac{n_F(-\xi_{k,i}) + n_B(\epsilon_{k',i'})}{\omega + i0^+ - \xi_{k,i} - \epsilon_{k',i'}} \right] \hat{U}_{f,i,l}^*(\mathbf{k}) \hat{U}_{X,i',l}(\mathbf{k}') \quad (17) \end{aligned}$$

with $\hat{U}_f(\mathbf{k})$ and $\hat{U}_X(\mathbf{k})$ being the unitary matrices that diagonalize the mean field Hamiltonian $\hat{h}_f(\mathbf{k})$ and $\hat{h}_X(\mathbf{k})$ respectively. Here k, l represent the matrix element index in $\hat{G}_\sigma^R(\omega, \mathbf{k}, \mathbf{k}')$. The subscripts i, i' denote the i th and i' th eigenvalues of $\hat{h}_f(\mathbf{k})$ and $\hat{h}_X(\mathbf{k})$, respectively. The QSL electronic DOS in the lattice model is then derived to be

$$\rho_\sigma(\omega, B, 0) = -\frac{1}{N^2\pi} \sum_{k,k'} \text{trIm} \hat{G}_\sigma^R(\omega, \mathbf{k}, \mathbf{k}'). \quad (18)$$

The computation of Eq. (17) is extremely heavy when the magnetic unit cell has a large size in a small magnetic flux. In the simulation, we take the magnetic flux ratio to be $\phi = 1/9$, which is the limit of our computing power. Given $\phi = 1/9$, the spinon DOS calculated from Eq. (16) is plotted as the blue line in Fig. 4(a). It can be seen that the continuous spinon DOS at $\phi = 0$ is discretized into nine peaks. The spinon band in Eq. (11) deviates from the quadratic dispersion in high energy, so the Landau discretized peaks in Fig. 4(a) are not uniformly distributed. The corresponding QSL electronic DOS calculated from Eqs. (17) and (18) at $\phi = 1/9$ is plotted as the blue line in Fig. 4(c), where one can see clearly that eight steps emerge near the Hubbard band edges. As labeled in Fig. 4(c), each step corresponds to one discrete peak in the spinon DOS. In Fig. 4(c), the step from the zeroth peak in Fig. 4(a) is merged into the bulk LHB, so

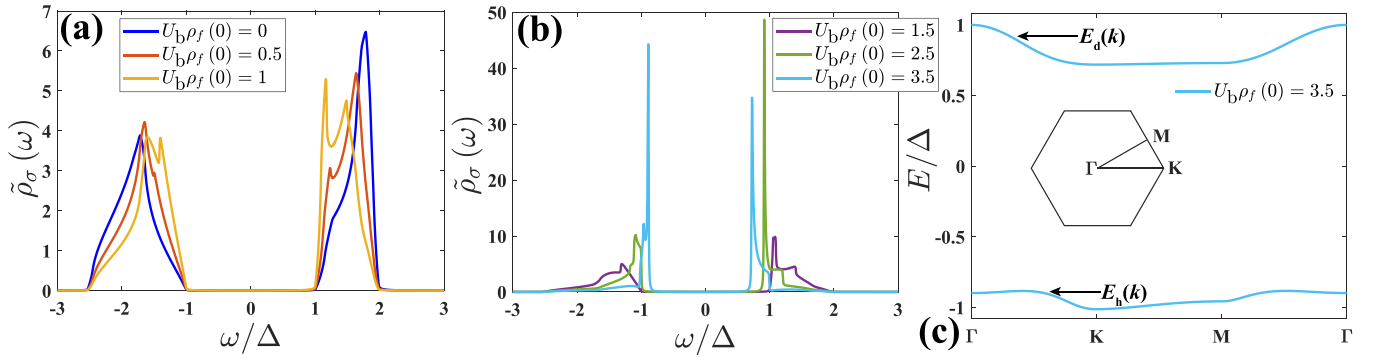


FIG. 5. (a) The QSL electronic DOS in different gauge-binding interactions at $B = 0$ T. A pair of band-edge resonance peaks develop as the gauge binding $U_b\rho_f(0)$ increases from 0 to 1. (b) The evolution of the band edge resonance peaks as the gauge binding $U_b\rho_f(0)$ further increases. Given a sufficiently large gauge binding, the band edge resonance peaks move inside the Mott gap and become in-gap peaks. The pair of in-gap peaks at $U_b\rho_f(0) = 3.5$ indicate a pair of in-gap bound states. (c) The band dispersions of the in-gap bound states formed at $U_b\rho_f(0) = 3.5$. The inset denotes the Brillouin zone of the triangular lattice. Here the binding equations in Eqs. (21) and (22) are solved in zero temperature.

it is difficult to identify. The step from the seventh spinon LL gets mixed with that from the eighth spinon LL because of the small energy spacing between the two spinon LLs. Physically, each edge step emerging in the QSL electronic DOS indicates a sudden change in the number of electronic states as the integer part of the spinon LL filling factor ν changes by 1. Those steps reflect the electron fractionalization in the QSL. In sharp contrast to the edge steps emerging in the QSL electronic DOS, the electronic DOS of a band insulator in an orbital magnetic field always shows discrete Dirac Delta function like peaks inside the bands, as schematically shown in the inset of Fig. 4(c). The discrete peaks in the Fig. 4(c) inset originate from the electronic LLs inside the bands. In the presence of an orbital magnetic field, such completely different features between the electronic DOS of a QSL and a band insulator therefore provide a further diagnosis to the ground state of an insulator that exhibits QOs. The edge steps in the QSL electronic DOS are regarded as a unique feature that characterizes Landau quantization of the in-gap neutral Fermi surfaces.

V. SPINON CHARGON ATTRACTION: CASE OF ZERO MAGNETIC FIELD

In a $U(1)$ QSL, the spinon and the chargon that are fractionalized from an electron both couple to an emerging $U(1)$ gauge field [8,45], so fluctuations of the $U(1)$ gauge field in turn affect the composite electronic state. For a gapless $U(1)$ QSL in an orbital magnetic field, it has been predicted in Secs. III and IV that the QSL electronic DOS is characterized by a few steps emerging near the Hubbard band edges, so one question to ask is how those steps evolve as the gauge field fluctuations are turned on. In this section, we first proceed with the case of zero magnetic field.

Near the band edge energies $\omega = \pm\Delta$, the longitudinal component of the gauge field fluctuations is supposed to have a dominant effect [22–24] because the transverse components of the gauge field fluctuations are negligible due to the small current-current correlations there. The longitudinal

gauge field fluctuations generate a gauge-binding interaction U_b [22,46] that couples the spinon and the chargon,

$$H_{\text{int}} = \frac{U_b}{N} \sum_{\sigma, k, q, q'} f_{\sigma, k-q}^\dagger f_{\sigma, k-q'} (a_{-q} a_{-q'}^\dagger - b_q^\dagger b_{q'}), \quad (19)$$

so the mean-field Hamiltonian for the QSL becomes $H = H_0 + H_{\text{int}}$. The original gauge binding interaction is like a Coulomb interaction, but the itinerant spinons can screen the gauge binding and make it a short-range on-site interaction. The gauge-binding interaction strength depends on the screening of the SFS [41]. The gauge-binding interaction U_b changes the QSL electronic DOS to be [41]

$$\tilde{\rho}_\sigma(\omega) = -\frac{1}{N\pi} \sum_k \text{Im} \frac{\frac{1}{N} \sum_q G_{h,\sigma}^R(\omega, \mathbf{k}-\mathbf{q}, \mathbf{q})}{1 - \frac{U_b}{N} \sum_q G_{h,\sigma}^R(\omega, \mathbf{k}-\mathbf{q}, \mathbf{q})}} - \frac{1}{N\pi} \sum_k \text{Im} \frac{\frac{1}{N} \sum_q G_{d,\sigma}^R(\omega, \mathbf{k}-\mathbf{q}, \mathbf{q})}{1 + \frac{U_b}{N} \sum_q G_{d,\sigma}^R(\omega, \mathbf{k}-\mathbf{q}, \mathbf{q})}}, \quad (20)$$

where $G_{h,\sigma}^R(\omega, \mathbf{k}, \mathbf{k}')$ and $G_{d,\sigma}^R(\omega, \mathbf{k}, \mathbf{k}')$ are the retarded Green's function for the states in the LHB and UHB, respectively. The expressions of $G_{h,\sigma}^R(\omega, \mathbf{k}, \mathbf{k}')$ and $G_{d,\sigma}^R(\omega, \mathbf{k}, \mathbf{k}')$ are given in the first and second terms in Eq. (3), respectively.

For the gapless $U(1)$ QSL in the triangular lattice, the QSL electronic DOS at the gauge binding $U_b\rho_f(0) = 1$ is plotted in Fig. 5(a). Here $\rho_f(0) = \rho_{f,\uparrow}(0) + \rho_{f,\downarrow}(0)$ denotes the total spinon DOS at the spinon Fermi level. The value $U_b\rho_f(0) = 1$ is an ideal case where the SFS brings about a Thomas-Fermi type screening [41]. In Fig. 5(a), it is observed that as the gauge-binding interaction increases from zero, a pileup of spectral weight is transferred from the bulk Hubbard bands to the band edges, which eventually gives rise to a pair of band edge resonance peaks. The DOS spectra is similar to that of a magnetic impurity embedded in a QSL, but a larger gauge binding is required to have a pair of band edge resonance peaks induced in the pristine QSL [30,46]. Physically, the gauge-binding $U_b\rho_f(0) = 1$ promotes the binding of a spinon hole and a holon to form a hole state and also the binding of a spinon and a doublon to form an electronic state, but

$U_b \rho_f(0) = 1$ is not sufficiently large to generate real bound states. Therefore, the pair of band edge resonance peaks at $U_b \rho_f(0) = 1$ in Fig. 5(a) represent the precursors of the bound states. When the gauge binding interaction increases, the band edge resonance peaks are found to further move towards the Mott gap, as can be seen in Fig. 5(b). Given a sufficiently large gauge binding $U_b \rho_f(0) = 3.5$, the peaks in the QSL electronic DOS are mainly localized inside the Mott gap. The in-gap peaks in Fig. 5(b) indicate the formation of real in-gap bound states at $U_b \rho_f(0) = 3.5$. Importantly, the bound states are in-gap itinerant electronic states that have band dispersions. The binding equations that determine the band dispersions of the bound states are derived to be [41]

$$\frac{1}{U_b} - \frac{A_c}{(2\pi)^2} \int \frac{n_F(\xi_{\mathbf{k}-\mathbf{q}}) + n_B(\epsilon_q)}{E_h(\mathbf{k}) + i0^+ - \xi_{\mathbf{k}-\mathbf{q}} + \epsilon_q} d^2\mathbf{q} = 0, \quad (21)$$

$$\frac{1}{U_b} + \frac{A_c}{(2\pi)^2} \int \frac{n_F(-\xi_{\mathbf{k}-\mathbf{q}}) + n_B(\epsilon_q)}{E_d(\mathbf{k}) + i0^+ - \xi_{\mathbf{k}-\mathbf{q}} - \epsilon_q} d^2\mathbf{q} = 0, \quad (22)$$

where $E_h(\mathbf{k})$ and $E_d(\mathbf{k})$ are the band dispersions of the hole bound state above the LHB and the electronic bound state below the UHB, respectively. The bound state bands at $U_b \rho_f(0) = 3.5$ solved from Eqs. (21) and (22) are plotted in Fig. 5(c). There are two Van Hove singularities in $E_h(\mathbf{k})$ and one in $E_d(\mathbf{k})$, so the electronic DOS shows two peaks in $\omega < 0$ and one in $\omega > 0$. Near Γ , the band $E_h(\mathbf{k})$ shows a flipped Mexican-hat-like shape, while the band $E_d(\mathbf{k})$ is quadratic with a negative effective mass. The two shapes of bound state bands shown in Fig. 5(c) are quite representative for the spinon chargon bound states. In fact, the specific bound state band shape is affected by many factors such as the gauge binding strength, the dispersions of the spinon and chargon bands, the spinon chemical potential, and temperature, etc. In Sec. VII below, the bound state band shape is further analyzed in the continuum model near Γ .

VI. WEAK SPINON CHARGON BINDING IN A MAGNETIC FIELD: BAND EDGE RESONANCE PEAKS

Given a weak gauge-binding interaction that arises from the $U(1)$ gauge field fluctuations, it has been found in Sec. V that the QSL electronic DOS at $B = 0$ T has a pair of resonance peaks that develop at the Hubbard band edges. In the presence of a finite orbital magnetic field, when the magnetic flux ratio $\phi = \frac{eB}{h} \frac{\sqrt{3}a^2}{2}$ is rational, we can proceed to deal with the gauge-binding effect in the lattice model. In the lattice model of a QSL that couples with an orbital magnetic field, the gauge-binding term in Eq. (19) is changed to be

$$\hat{H}_{\text{int}} = \frac{U_b}{N'} \sum_{\sigma, \mathbf{k}, \mathbf{q}, \mathbf{q}', i} \hat{f}_{\sigma, \mathbf{k}-\mathbf{q}, i}^\dagger \hat{f}_{\sigma, \mathbf{k}-\mathbf{q}', i} (\hat{a}_{-\mathbf{q}, i} \hat{a}_{-\mathbf{q}', i}^\dagger - \hat{b}_{\mathbf{q}, i}^\dagger \hat{b}_{\mathbf{q}', i}), \quad (23)$$

where subscript i labels the i th elements in the column vectors $\hat{a}_{-\mathbf{k}}$, $\hat{b}_{\mathbf{k}}$, and $\hat{f}_{\sigma, \mathbf{k}}$. Here $N' = N/I$ is the number of magnetic unit cells and I is the number of lattice sites in one magnetic unit cell. Now the QSL mean-field Hamiltonian becomes $\hat{H} = \hat{H}_0 + \hat{H}_{\text{int}}$. For the QSL with multiple spinon and chargon bands, the gauge-binding interaction U_b changes the

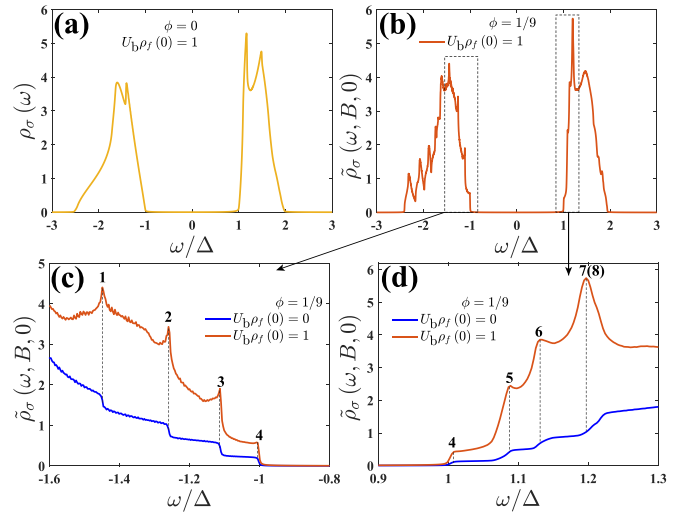


FIG. 6. (a) The QSL electronic DOS at $U_b \rho_f(0) = 1$ in zero magnetic flux. (b) The QSL electronic DOS at $U_b \rho_f(0) = 1$ with the magnetic flux ratio being $\phi = 1/9$. At both the LHB top and the UHB bottom, the electric DOS spectra in (b) shows a few resonance peaks. (c), (d) Zoom-in of the DOS spectra in the black dashed rectangles in (b). The electronic DOS $\rho_\sigma(\omega, B, 0)$ at $\phi = 1/9$ with zero gauge binding is plotted in blue for comparison. The resonance peaks at the Hubbard band edges are found to appear at the same energies as those of the edge steps in the electronic DOS $\rho_\sigma(\omega, B, 0)$. It indicates that in an orbital magnetic field, each edge step at zero U_b in the QSL electronic DOS evolves into a resonance peak in the presence of weak gauge interaction U_b .

QSL electronic DOS in Eq. (18) to be [41]

$$\begin{aligned} \tilde{\rho}_\sigma(\omega, B, 0) = & -\frac{1}{N\pi} \sum_{\mathbf{k}} \text{trIm} \left\{ \left[\frac{1}{N} \sum_{\mathbf{q}} \hat{G}_{h,\sigma}^R(\omega, \mathbf{k} - \mathbf{q}, \mathbf{q}) \right] \right. \\ & \times \left. \left[1 - \frac{U_b}{N'} \sum_{\mathbf{q}} \hat{G}_{h,\sigma}^R(\omega, \mathbf{k} - \mathbf{q}, \mathbf{q}) \right]^{-1} \right\} \\ & - \frac{1}{N\pi} \sum_{\mathbf{k}} \text{trIm} \left\{ \left[\frac{1}{N} \sum_{\mathbf{q}} \hat{G}_{d,\sigma}^R(\omega, \mathbf{k} - \mathbf{q}, \mathbf{q}) \right] \right. \\ & \times \left. \left[1 + \frac{U_b}{N'} \sum_{\mathbf{q}} \hat{G}_{d,\sigma}^R(\omega, \mathbf{k} - \mathbf{q}, \mathbf{q}) \right]^{-1} \right\}, \quad (24) \end{aligned}$$

where the elements of the retarded Green's function matrix $\hat{G}_{h,\sigma}^R(\omega, \mathbf{k}, \mathbf{k}')$ and $\hat{G}_{d,\sigma}^R(\omega, \mathbf{k}, \mathbf{k}')$ are given by the first and second terms in Eq. (17), respectively.

In the weak gauge-binding $U_b \rho_f(0) = 1$, the QSL electronic DOS at $\phi = 0$ and $\phi = 1/9$ are plotted in Figs. 6(a) and 6(b), respectively. The electronic DOS spectra of $\phi = 1/9$ has a similar shape as that of $\phi = 0$, but more band edge resonance peaks appear in the spectra of $\phi = 1/9$ in Fig. 6 (b). The band edge resonance peaks near the LHB top and the UHB bottom are zoomed in Fig. 6(c) and 6(d) respectively, with the electronic DOS spectra $\rho_\sigma(\omega, B, 0)$ at

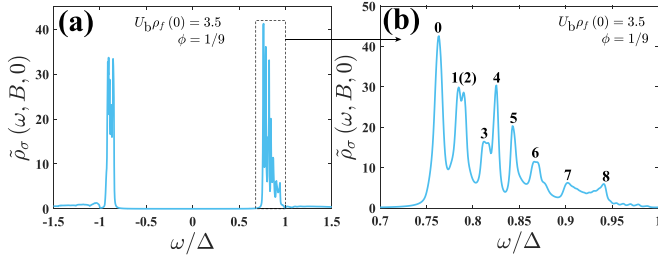


FIG. 7. (a) The QSL electronic DOS at $U_b \rho_f(0) = 3.5$ with the magnetic flux being $\phi = 1/9$. As the gauge binding is sufficiently large to induce real in-gap bound states, the electronic DOS is composed of in-gap peaks that originate from the bound state LLs. (b) Zoom-in of black dashed rectangle in (a). The discrete peaks indicate Landau quantization of the electronic bound state below the UHB. Given the magnetic flux $\phi = 1/9$, there are nine bound-state LLs as labeled.

$\phi = 1/9$ in Fig. 2(c) plotted for comparison. From Figs. 6(c) and 6(d), one can find that the weak gauge binding $U_b \rho_f(0) = 1$ evolves each Hubbard band edge step into a resonance peak. Physically, since the gauge binding U_b tends to bind spinon LL states with chargons, each resonance peak near the LHB band edge in Fig. 6(c) corresponds to the quasibinding of a spinon hole LL state and a holon. Similarly, each resonance peak near the UHB band edge in Fig. 6(d) indicates a quasibound state of a spinon LL state and a doublon. As a result, in an orbital magnetic field, both the weak gauge binding induced multiple band edge resonance peaks and the emerging band edge steps at zero gauge binding have the intrinsic connection to the spinon LLs, as labeled in Figs. 6(c) and 6(d).

In the weak gauge binding $U_b \rho_f(\omega) = 1$, each resulting band edge resonance peak appears almost at the same energy as that of the band edge step at $U_b \rho_f(\omega) = 0$. When the applied orbital magnetic field B changes, the energy spacing between the adjacent band edge resonance peak in Figs. 6(b) and 6(c) changes linearly with B . In the weak gauge binding regime, since the loosely quasibound spinon chargin pairs have a negligible energy change, the energy dependence of the band edge resonance peaks on B follows that of the spinon LLs. In the strong gauge binding regime, all the band edge resonance peaks move inside the Mott gap and evolve into in-gap peaks as shown in Figs. 7(a) and 7(b). Those in-gap peaks originate from the in-gap bound state LLs. Since real in-gap bound states are formed, the energy saved in the binding, namely, the binding energy, plays an important role in determining the bound-state energy. In contrast to the linear B energy dependence of the band edge resonance peaks in the weak gauge binding regime, the interplay between the binding energy and the orbital magnetic field B in the strong gauge binding regime complicates the B dependence of the in-gap bound state LL spectrum.

VII. STRONG SPINON CHARGON BINDING IN A MAGNETIC FIELD: BOUND STATE BAND DISPERSIONS AND THE LANDAU LEVELS

To get the in-gap bound state LL spectrum, the bound-state band dispersions in $B = 0$ T need to be analyzed first. In the

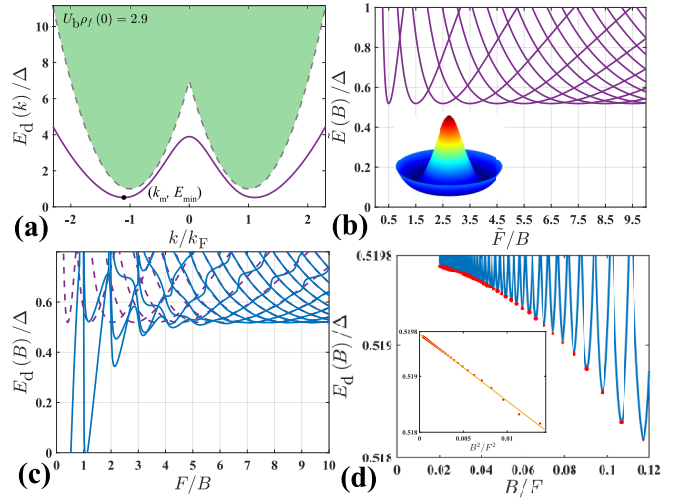


FIG. 8. (a) The electronic bound state band dispersion numerically solved from Eq. (27). A Mexican-hat-like bound-state band dispersion emerges from the threshold energy $E_{th}(k)$ that is denoted by the black dashed line. The black dot on the bound-state band denotes the bound-state band minimum E_{min} at $|k| = k_m$. The green shaded region corresponds to the continuous spectrum of the electronic excitations in the UHB. (b) The LL spectrum of a charged particle that has the same band dispersion $E(k) = E_d(k)$ as shown in (a). The inset in the lower left corner shows the two-dimensional plot of the bound state band in (a), which has the shape of a Mexican hat. Note that the gap is periodically modulated in $1/B$. (c) The LL spectrum of the electronic bound state with the band dispersion shown in (a). The LL spectrum is numerically solved from Eq. (27). The LL spectrum in (b) is plotted as purple dashed lines for comparison. At $B \rightarrow 0$, the electronic LLs $E_{d,n}(B)$ approaches $\tilde{E}_n(B)$. (d) The electronic bound state LL spectrum in (c) plotted as a function of B/F . The minimum of each LL is labeled by a red dot, and the red dots are plotted in B^2/F^2 in the inset. In the inset, the minimum values of LLs exhibit the linearly decrease in B^2/F^2 , which indicates that the envelop energy of the electronic bound-state LL spectrum decreases quadratically in B . Here the temperature has been fixed to be $k_b T / \mu_f = 0.05$ in all the calculations.

strong gauge binding regime, a spinon hole gets bound with a holon to form a hole bound state above the LHB, while an electronic bound state below the UHB arises from the binding of a spinon and a doublon. The binding process of a spinon hole and a holon is similar to that of a spinon-doublon bound state, so in the below we mainly focus on the electronic bound state formed by a spinon and a doublon. The binding of a spinon hole and a holon can be found in the Supplemental Material [41].

A. The Mexican-hat-like band dispersion

To proceed, we consider the continuum model near Γ , where the spinon band and the chargin band are approximated by the quadratic dispersions: $\xi_k = \frac{\hbar^2 k^2}{2m_f} - \mu_f$ and $\epsilon_k = \frac{\hbar^2 k^2}{2m_x} + \Delta$, respectively. In the continuum description of the gapless $U(1)$ QSL, the threshold energy to excite an electron with a quasimomenta \mathbf{k} is $E_{th}(\mathbf{k}) = \frac{\hbar^2 (|\mathbf{k}| - |\mathbf{k}_F|)^2}{2m_x} + \Delta$ [41], where \mathbf{k}_F is the spinon Fermi wave vector. In Fig. 8(a), the black dashed line denotes the threshold energy $E_{th}(\mathbf{k})$, and the green shaded

region above $E_{\text{th}}(\mathbf{k})$ corresponds to the continuous electronic excitation spectrum. In the presence of a sufficiently large gauge binding, an electronic state gets dragged down and becomes a bound state with the band dispersion just below $E_{\text{th}}(\mathbf{k})$. In the continuum description, the electronic bound state binding equation in Eq. (22) is changed to be

$$\frac{1}{U_b} + \frac{A_c}{(2\pi)^2} \int_0^{|q|=k_c} \frac{n_F(-\xi_{\mathbf{k}-q}) + n_B(\epsilon_q)}{E_d(\mathbf{k}) + i0^+ - \xi_{\mathbf{k}-q} - \epsilon_q} d^2q = 0, \quad (25)$$

with k_c being the momenta cutoff. Given the band parameters $m_f/m_X = 3$, $\Delta/\mu_f = 1/2$, $U_b\rho_f(0) = 2.9$, and the cutoff $k_c = 2.6|k_F|$, one gets the electronic bound state band with a Mexican hat like dispersion shown in Fig. 8(a). The evolution of the electronic bound state band as the gauge-binding interaction increases can be found in Fig. S2 in the Supplemental Material [41]. The Mexican-hat-like shape of the electronic bound state band is inherited from the threshold energy $E_{\text{th}}(\mathbf{k})$, and it is one representative bound state band dispersion.

To get the LL spectrum of the electronic bound state with the band dispersion $E_d(\mathbf{k})$, it is instructive to first consider Landau quantization of a free charged particle with a general energy dispersion $E(\mathbf{k})$ that depends on k^2 only. It is straightforward to show that a simple substitution $k^2 = 2l_B^{-2}(n + \frac{1}{2})$ [41] gives the n th LL $\tilde{E}_n(B) = E[\sqrt{2l_B^{-2}(n + \frac{1}{2})}]$ of the free charged particle. Here $l_B = \sqrt{\frac{\hbar}{eB}}$ is the magnetic length. For the Mexican-hat-like band dispersion shown in Fig. 8(a), the corresponding spectrum $\tilde{E}_n(B)$ is plotted in Fig. 8(b). Importantly, for a Mexican-hat-like band $E(\mathbf{k}) = E_d(\mathbf{k})$ that takes the band minimum at $|\mathbf{k}| = k_m$, the resulting spectrum $\tilde{E}_n(B)$ takes the same minimum value at $1/B = \frac{2\pi e}{\hbar\pi k_m^2}(n + \frac{1}{2})$ with $n = 0, 1, 2, \dots$. Therefore, the edge of the spectrum $\tilde{E}_n(B)$ oscillates in $1/B$, as can be seen in Fig. 8(b). The oscillation frequency is $\tilde{F} = \frac{\pi\hbar k_m^2}{2\pi e}$, where the wave vector at the band minimum plays the role of the Fermi wave vector in a metal. The constant band minimum E_{min} defines the envelop of the band edge oscillation.

Interestingly, the LL spectrum $\tilde{E}_n(B)$ of a free charged particle indicates that for insulating systems with a Mexican-hat-like conduction or valence band, the resulting LL spectrum would induce insulating gap modulations so the thermally activated resistivity oscillates with B . The oscillation of the resistivity ratio to the background resistivity is detectable even at low temperatures [20,21]. An example of this kind of Mexican-hat-like band may be found in the biased Bernal bilayer graphene [47]. It will be interesting to search for this effect experimentally. This provides another mechanism for observing QOs in band insulators, because, unlike previous proposals, the gap is not generated by hybridization [18–21].

B. Landau quantization of the in-gap bound state

The spectrum $\tilde{E}_n(B)$ obtained through the simple substitution cannot give the correct LLs of the electronic bound state that is composed of a spinon and a doublon in the QSL. For the electronic bound state formed in an orbital magnetic field, the magnetic field is divided into two parts acting on the spinons

and the doublons, respectively. The effect of the orbital magnetic field is twofold. First, the constituent particles, namely, the spinons and the doublons, all have the LLs formed in the spectrum, which increase their energy. Thus, the energy of the composite particle is expected to increase. Second, the wave functions of the spinons and doublons become more localized, which tend to increase the binding energy, leading to a decrease of the energy of the composite particle. Therefore, these two effects tend to compete. As a result, the bound-state Landau quantization is a much more complicated problem that we will deal with below.

For the gapless $U(1)$ QSL in an orbital magnetic field B , the gauge binding occurs between the spinon LL states and the chargin LL states. In the LL basis, the gauge-binding term takes the form

$$\begin{aligned} H_{\text{int}}(b, B - b) &= \sum_{\sigma, n_1, n_2, n'_1, n'_2, m_1, m_2, m'_1, m'_2} \tilde{U}_{b, n_1, n_2, n'_1, n'_2, m_1, m_2, m'_1, m'_2} \\ &\times f_{n_1, m_1, \sigma}^\dagger f_{n_2, m_2, \sigma} (a_{n'_1, m'_1}^\dagger a_{n'_2, m'_2}^\dagger - b_{n'_1, m'_1}^\dagger b_{n'_2, m'_2}^\dagger), \quad (26) \end{aligned}$$

with the interaction matrix elements given in the Supplemental Material [41]. In principle, the LL spectrum of the bound states can be obtained through diagonalizing the mean-field Hamiltonian $H(b, B - b) = H_0(b, B - b) + H_{\text{int}}(b, B - b)$. However, it is extremely challenging to fully diagonalize $H(b, B - b)$ given an arbitrary magnetic field partition. In the weak Mott regime of the QSL, since the EGMF b dominates over the remaining $B - b$, we proceed with the limiting case of $b \rightarrow B$. Calculations about the bound state LL spectrum in the opposite limiting case of $b \rightarrow 0T$ can be found in the Supplemental Material [41].

The limiting case offers great simplification because the kernel of the integral equation factorizes, leading to the much simpler binding equation below for the electronic bound state energies $E_{d,n}(B)$ [41]:

$$\begin{aligned} \frac{1}{U_b} + \frac{A_c}{(2\pi)^2} \sum_{n'} \int_0^{|q|=k_c} \frac{n_F(-\xi_{n'}) + n_B(\epsilon_q)}{E_{d,n}(B) + i0^+ - \xi_{n'} - \epsilon_q} \\ \times D_{n,n'}(q) D_{n',n}(-q) \exp(-l_B^2 q^2 / 2) d^2q = 0. \quad (27) \end{aligned}$$

Here the function $D_{n,n'}(q)$ respects the relation $D_{n,n'}(q) = D_{n',n}(-q^*)$ and its expression for $n \geq n'$ is $D_{n,n'}(q) = \sqrt{n! / n'!} (-l_B q / 2)^{n-n'} L_{n-n'}^{n-n'}(l_B^2 q q^* / 2)$ with $q = q_x + i q_y$. The function $L_n^m(x)$ is the associated Laguerre function. The binding equation for the hole bound state can be found in the Supplemental Material [41].

By numerically solving Eq. (27), the resulting LL spectrum $E_{d,n}(B)$ that correspond to the bound state dispersion in Fig. 8(a) is plotted in Figs. 8(c) and 8(d). It can be seen in Fig. 8(c) that the band edge of $E_{d,n}(B)$ oscillates in $1/B$ as well. In the small magnetic field region, the electronic bound state LL spectrum $E_{d,n}(B)$ approaches the spectrum $\tilde{E}_n(B)$ as $B \rightarrow 0T$. As the magnetic field increases, the band edge oscillation of $E_{d,n}(B)$ intensifies and the frequency approaches to $F = \frac{\pi\hbar k_F^2}{2\pi e}$, which equals the oscillation frequency of the

spinon chemical potential $\mu_f(b=B)$ [41]. It is consistent with the fact that the memory of the spinon chemical potential oscillation is retained after forming the bound state, so the band-edge oscillation of $E_{d,n}(B)$ originates intrinsically from Landau quantization of the SFS.

Importantly, the envelop energy of $E_{d,n}(B)$ is found to decrease quadratically with B as seen in Fig. 8(d), indicating an increase in the binding energy. We believe that the reason behind it is the orbital magnetic field effect on the binding energy. In the limit of $b \rightarrow B$ we considered, the orbital magnetic field B only acts on the spinons. The magnetic field on the spinons induces the spinon chemical potential to oscillate and makes the spinon wave function more and more localized as B increases. Intuitively, binding a doublon with a more spatially localized spinon is energetically more favorable, so the binding energy increases as B increases. The increase of the binding energy brings down the electronic bound-state energy. In a finite temperature, the binding energy at finite B must be smoothly connected to that at $B=0T$, so a quadratic B term, which is the lowest allowed order, must be involved in the binding energy. For the electronic bound state with a Mexican-hat-like band dispersion, when the effect of the orbital magnetic field on the binding energy is not considered, the envelop energy of the spectrum $\tilde{E}_n(B)$ is the constant E_{\min} . After the quadratic B -dependent binding energy is taken into account, it introduces a term that decreases quadratically in B to the electronic bound-state energy, so the resulting envelop energy of the electronic bound state LL spectrum solved from Eq. (27) exhibits the quadratic decrease in B .

It is important to note that the quadratic decrease of the electronic bound-state envelop energy in B is unique to the bound state that has a Mexican-hat-like band dispersion at $B=0T$. In fact, the quadratic decrease of the envelop energy of the bound state with B stems from two indispensable factors: one is the quadratic increase of the binding energy in B ; the other is the constant envelop energy E_{\min} of the spectrum $\tilde{E}_n(B)$. To demonstrate this point, we consider the case where the electronic bound state has a quadratic band dispersion shown in Fig. 9(a). This occurs by tuning U_b . As shown in Fig. 9(b), the bound-state LL spectrum $E_{d,n}(B)$ approaches $\tilde{E}_n(B)$ as $B \rightarrow 0T$. For the bound state in Fig. 9(a), since all the energy levels in $\tilde{E}_n(B)$ increase linearly in B , in the $B \rightarrow 0T$ regime, the linear B increase dominates over the quadratic B -dependent term in the binding energy. As a result, the LL spectrum $E_{d,n}(B)$ of an electronic bound state with a quadratic band dispersion retains the linear B increase in the $B \rightarrow 0T$ regime, as can be seen in Fig. 9(b). As B further increases, the band edge of the LL spectrum $E_{d,n}(B)$ starts to show the oscillation that comes from the spinon chemical potential oscillation. Interestingly, in Fig. 9(b) the envelop energy of the oscillation is seen to change from increasing in B to decreasing in B as B continues increasing, indicating that the orbital magnetic field promoted energy saving in the binding finally becomes dominant. It again matches the intuition that the binding saves more energy as B increases, regardless of the resulting bound-state band dispersion. The above analysis on the electronic bound state LL spectrum applies to the hole bound-state LL spectrum as well [41].

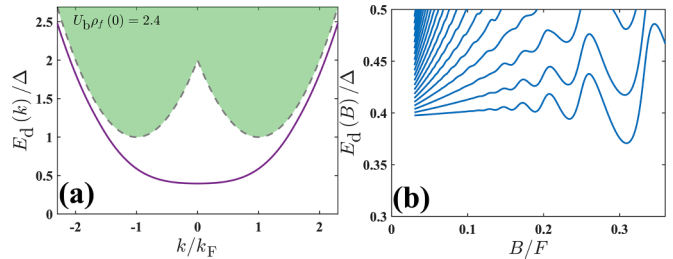


FIG. 9. (a) The electronic bound state band with a quadratic dispersion. The band parameters used in solving Eq. (25) are $m_f/m_x = 1/2$, $\Delta/\mu_f = 1/2$, $U_b\rho_f(0) = 2.4$, $k_bT/\mu_f = 0.05$. The momenta cut-off is set to be $k_c = 2.6|k_F|$. (b) The LL spectrum corresponding to the electronic bound state band shown in (a). In the region $B \rightarrow 0T$, the electronic bound state energy levels exhibit the linear increase in B . As the magnetic field B increases, the bound state energy levels start to show the oscillation that originates from the spinon chemical potential oscillation. When the magnetic field B is sufficiently large, the envelop energy of the oscillation turns to decrease in B because the orbital magnetic field induced energy saving plays the dominant role in the binding.

VIII. CONNECTION TO EXPERIMENTS

We have studied the effects of orbital magnetic field and gauge field fluctuations on the electronic DOS of the $U(1)$ QSL with SFS. For the electronic DOS spectra, one widely used technique to detect the local electronic DOS in experiments is the STM. Given a simple metal as the STM tip, the differential conductance in the setup is [48]

$$\frac{dI}{dV} \propto \int_{-\infty}^{\infty} -\frac{\partial n_F(\omega + eV)}{\partial \omega} \sum_{\sigma} \tilde{\rho}_{\sigma}(\omega, b, B - b) d\omega, \quad (28)$$

where $\tilde{\rho}_{\sigma}(\omega, b, B - b)$ is the QSL electronic DOS that covers both the effects of orbital magnetic field and gauge binding. As analyzed in Secs. II and VI, the DOS spectra of a $U(1)$ QSL with SFS at $B=0T$ and $U_b\rho_f(0) = 0$ is composed of two domelike regions separated by a Mott gap as schematically illustrated in Fig. 10(a).

As mentioned in Sec. I, recent STM measurements on the bulk 1T-TaS₂, monolayer 1T-TaSe₂ [29–31], and 1T/1H-TaS₂ heterostructures [32] all show clear Hubbard band edges in the electronic DOS spectra. Specifically, on the surface of the layered 1T-TaS₂, an extra resonance peak with sidebands was found near the UHB edge [27]. In a subsequent measurement in an external magnetic field [33], the UHB edge resonance peak was found to move towards the Mott gap center as the magnetic field increases, and its energy exhibits a quadratic decrease with B . For the LHB edge, it was observed to move away from the Mott gap center, albeit at a much smaller rate. The evolution of the DOS spectra in an external magnetic field observed in the experiment [33] is schematically indicated in Fig. 10(a).

The experimental observation of the LHB edge and UHB edge resonance peak evolving in the same direction in an external magnetic field is a surprising result. It indicates that the energy cost to excite a hole increases with the external magnetic field but that to excite an electron decreases. Normally, we expect the electron energy to increase due to orbital effects of a magnetic field. Hence, the observation for

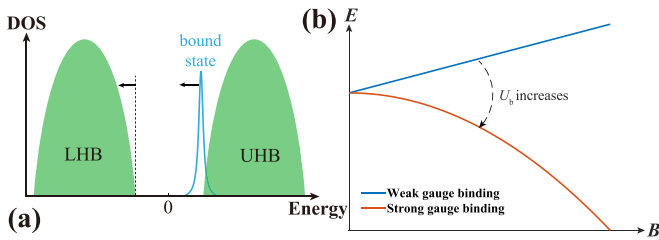


FIG. 10. (a) The schematic showing of the layered 1T-TaS₂ electronic DOS spectra measured in the experiment [27,33]. A resonance peak emerges at the UHB edge but no such resonance peak is observed at the LHB edge. By applying a magnetic field, the energy of the resonance peak is observed to decrease and so does that of the LHB edge, even though the effect on the LHB edge is much smaller. The direction of the shift of the UHB edge resonance peak and the LHB edge with the applied magnetic field is indicated by the black arrows. Importantly, the energy of the UHB edge peak exhibits a quadratic decrease with B in the experiment. (b) Schematic drawing of the theoretical prediction for the energy dependence of the UHB edge peak on the applied magnetic field. In the weak gauge binding regime, the energy of the UHB edge peak increases linearly as that of the spinon LL. In the strong gauge binding regime, the energy of the UHB edge peak is determined by the envelop energy of the bound state LL spectrum, so it decreases quadratically with B . As the gauge binding interaction increases, the UHB edge peak energy is expected to change from the linear increase with B to the quadratic decrease with B .

the UHB is highly surprising. We would like to interpret the DOS spectra observed in the experiment, assuming the material is a gapless $U(1)$ QSL. The UHB edge resonance peak is then interpreted as a quasibound state of a spinon and a doublon. In the experiment, the peak is accompanied by a series of sidebands which has been interpreted in analogy with phonon sidebands but using the amplitude mode of the charge density wave instead of phonons [27]. Note that in this scenario the electronic mode is usually required to be almost localized with a linewidth less than the phonon energy. This indicates that the electron is not in a propagating band, as the rather broad Hubbard band suggests. Instead, this fits our scenario that the electron is in a resonant or near bound state. Experimentally the spectral weight of the resonance and the sideband in the UHB is rather small. The weight may be comparable to the case $U_b\rho_f(0) = 1$ as shown in Figs. 5(a) and 6(a). This puts us in the intermediate binding regime where the state is not fully bound, but appears as a near edge resonance. Unfortunately, we do not have a quantitative theory for the orbital magnetic field induced evolution of the UHB edge resonance in this intermediate regime. Recall that in the strong binding regime, the LL spectrum of the real bound state with a Mexican-hat-like band dispersion has the envelop energy decrease quadratically with B , so the thermally smoothed peak of the bound state LLs is expected to have its energy decrease quadratically with B as well. For a general quasibound state near the UHB edge, the energy of the resonance peak therefore changes from the linear increase with B to the quadratic decrease with B as the gauge binding increases, which is schematically plotted in Fig. 10(b). By interpolating between the strong and weak binding limits, we may argue that the

behavior observed in the experiment is closer to the strong binding case ($U_b\rho_f(0) \sim [1.5, 3]$), and a B^2 decrease of the energy is expected. For the LHB edge, there is no resonance peak observed in the experiment at zero B , so the gauge binding of the spinon holes and the holons is presumably smaller. In a magnetic field, we predict an increase in the excitation energy, hence the threshold should move away from the gap center, in agreement with experiment. The B dependence is small and whether it is B^2 or not is less certain experimentally. Thus, qualitatively, a model based on spinon Fermi surface and spinon chargon binding may provide an explanation for the unusual features of the experiment: the existence of the side-bands and the magnetic field dependence.

In the layered 1T-TaS₂ electronic DOS spectra measured in the experiment [33], no Zeeman spin splitting was observed. The temperature in the measurement is $T = 1.5$ K and the largest applied magnetic field is $B = 12$ T. It is possible that the thermal fluctuations smear the spin split levels, so a spin-polarized STM measurement is needed to resolve the Zeeman effect. The thermal fluctuations may also be the reason why the band edge steps and multiple resonance peaks cannot be identified in the electronic DOS spectra in the magnetic field. In the current paper, we mainly focus on the orbital effects of the applied magnetic field. For the effect of Zeeman field, the electronic DOS spectra of the QSL with SFS is found to exhibit anomalous Zeeman shift: in the case of zero gauge binding, the threshold energy in the DOS spectra shows no Zeeman shift; in the weak gauge binding regime, the Zeeman field induced energy shift of the quasibound spinon chargon pairs is reduced; in the strong gauge binding regime, the Zeeman field shifts the bound states in the opposite direction to that in the standard Zeeman shift. The detailed study of the Zeeman field effect on the QSL with SFS is present in our companion paper [49].

In this paper, the QSL electronic DOS features of the Hubbard band edge steps and resonance peaks in a magnetic field are both found to have an intrinsic connection to the spinon LLs induced by the EGMF b on the spinons. In reality, the remaining $B - b$ on the chargons induces LLs as well, but the DOS features from the spinon LLs will always be maintained as long as the LL spacing respects $\hbar\omega_f \gg \hbar\omega_x$. To have the DOS features of band edge steps and resonance peaks well identified in the measurements, the temperature should lie in the range $k_bT \ll \hbar\omega_f$. The spinon bandwidth is set by the exchange scale, which is much smaller than the usual Fermi energy. However, in cases such as 1T-TaS₂, 1T-TaSe₂, and the organics, the unit cell size is large, making the spinon effective mass m_f a bit larger than the free electron mass m_e . Assuming the spinon effective mass to be $m_f \approx 2m_e$, one can find that the spinon LL spacing in $b \rightarrow B = 1$ T is 0.06 meV. In an experimental accessible magnetic field $B = 10$ T, the suitable temperature range to carry out the STM measurement is then estimated to be $k_bT/\hbar\omega_f < 1/10$, which gives $T < 0.7$ K. To identify the DOS features at the Hubbard band edges in the spectroscopy, a resolution better than 0.6 meV is required.

In the DOS spectra, each step or resonance peak near the Hubbard band edges is intrinsically connected to one spinon LL. However, it is not always true that each spinon LL can have a corresponding step or resonance peak emerging near the Hubbard band edges. The QSL simulated in a triangular

lattice in Sec. IV already shows in Fig. 4(c) that the zeroth spinon LL, which is the farthest one from the spinon chemical potential, has the corresponding step merged inside the bulk LHB and cannot be identified in the spectrum. By comparing Figs. 2(d) and 3(e), one can find that the prerequisite to have all the steps or resonance peaks from the spinon LLs identified at the Hubbard band edges is that the chargin bandwidth is larger than the energy between the farthest spinon LL and the spinon chemical potential, namely, $\Lambda_X - \Delta < \text{Min}[\Lambda_f + \mu_f, \Lambda_f - \mu_f]$.

IX. CONCLUSIONS

In this paper, we have studied the electronic DOS of a $U(1)$ QSL in an orbital magnetic field. The QSL electronic DOS spectra is found to have the characteristic Hubbard band edge steps induced by the spinon Landau quantization in the magnetic field. The band edge steps are further found to evolve into resonance peaks when the $U(1)$ interaction between spinons and chargons due to the weakly fluctuating gauge field is included. In an orbital magnetic field, the QSL electronic DOS features of the band edge steps and the resonance peaks behave completely differently from the discrete Delta like peaks in the DOS of a band insulator, so the finding provides a way to distinguish the QSL with neutral Fermi surfaces from a band insulator. In the case of strong $U(1)$

gauge field fluctuations, the large gauge binding can induce in-gap bound states and the LL spectrum of the in-gap bound states in a magnetic field are solved. For an in-gap bound state with a Mexican-hat-like band dispersion, the local DOS exhibits a peak which moves as B^2 towards the gap center with the magnetic field.

Recently, apart from the Mott physics in the 1T-TaS₂ and 1T-TaSe₂ family, other two-dimensional Mott insulating states have been reported in both the two-dimensional Moiré systems [50,51] and the monolayer 1T-NbSe₂ [52–55]. For those Mott insulators discovered recently, our study of the QSL electronic DOS spectra in an orbital magnetic field suggests that a tunneling measurement on the electronic DOS would serve as a great diagnosis to whether there exist neutral Fermi surfaces inside the insulating gap.

ACKNOWLEDGMENTS

The authors thank C. J. Butler and T. Hanaguri for sharing their unpublished data. W.-Y.H. thanks Yang Qi and Yuanbo Zhang for helpful discussions. W.-Y.H. acknowledges the start-up grant of ShanghaiTech University. P.A.L. acknowledges support by DOE office of Basic Sciences Grant No. DE-FG02-03ER46076. Part of the computing for this paper was performed on the HPC platform of ShanghaiTech University.

-
- [1] P. W. Anderson, The resonating valence band state in La₂CuO₄ and superconductivity, *Science* **235**, 1196 (1987).
 - [2] P. A. Lee, N. Nagaosa, and X.-G. Wen, Doping a Mott insulator: Physics of high-temperature superconductivity, *Rev. Mod. Phys.* **78**, 17 (2006).
 - [3] A. Yu. Kitaev, Fault-tolerant quantum computation by anyons, *Ann. Phys.* **303**, 2 (2003).
 - [4] C. Nayak, S. H. Simon, A. Stern, M. Freedman, and S. Das Sarma, Non-Abelian anyons and topological quantum computation, *Rev. Mod. Phys.* **80**, 1083 (2008).
 - [5] P. W. Anderson, Resonating valence bonds: A new kind of insulator? *Mater. Res. Bull.* **8**, 153 (1973).
 - [6] L. Savary and L. Balents, Quantum spin liquids: A review, *Rep. Prog. Phys.* **80**, 016502 (2017).
 - [7] Y. Zhou, K. Kanoda, and T.-K. Ng, Quantum spin liquid states, *Rev. Mod. Phys.* **89**, 025003 (2017).
 - [8] S.-S. Lee and P. A. Lee, U(1) Gauge Theory of the Hubbard Model: Spin Liquid States and Possible Application to κ -(BEDT-TTF)₂Cu₂(CN)₃, *Phys. Rev. Lett.* **95**, 036403 (2005).
 - [9] D. Podolsky, A. Paramekanti, Y. B. Kim and T. Senthil, Mott Transition Between a Spin-liquid Insulator and a Metal in Three Dimensions, *Phys. Rev. Lett.* **102**, 186401 (2009).
 - [10] O. I. Motrunich, Orbital magnetic field effects in spin liquid with spinon Fermi sea: Possible application to κ -(ET)₂Cu₂(CN)₃, *Phys. Rev. B* **73**, 155115 (2006).
 - [11] I. Sodemann, D. Chowdhury, and T. Senthil, Quantum oscillations in insulators with neutral Fermi surfaces, *Phys. Rev. B* **97**, 045152 (2018).
 - [12] D. Shoenberg, *Magnetic Oscillations in Metals* (Cambridge University Press, Cambridge, England, 1984).
 - [13] P. Wang, G. Yu, Y. Jia, M. Onyszczyk, F. A. Cevallos, S. Lei, S. Klimentz, K. Watanabe, T. Taniguchi, R. J. Cava, L. M. Schoop, and S. Wu, Landau quantization and highly mobile fermions in an insulator, *Nature (London)* **589**, 225 (2021).
 - [14] B. S. Tan, Y.-T. Hsu, B. Zeng, M. C. Hatnean, N. Harrison, Z. Zhu, M. Hartstein, M. Kiourlappou, A. Srivastava, M. D. Johannes, T. P. Murphy, J.-H. Park, L. Balicas, G. G. Lonzarich, G. Balakrishnan, and S. E. Sebastian, Unconventional Fermi surface in an insulating state, *Science* **349**, 287 (2015).
 - [15] Z. Xiang, Y. Kasahara, T. Asaba, B. Lawson, C. Tinsman, L. Chen, K. Sugimoto, S. Kawaguchi, Y. Sato, G. Li, S. Yao, Y. L. Chen, F. Iga, J. Singleton, Y. Matsuda, and L. Li, Quantum oscillations of electric resistivity in an insulator, *Science* **362**, 65 (2018).
 - [16] P. Czajka, T. Gao, M. Hirschberger, P. Lampen-Kelley, A. Banerjee, J. Yan, D. G. Mandrus, S. E. Nagler, and N. P. Ong, Oscillations of the thermal conductivity in the spin liquid state of α -RuCl₃, *Nat. Phys.* **17**, 915 (2021).
 - [17] Z. Xiang, K.-W. Chen, L. Chen, T. Asaba, Y. Sato, N. Zhang, D. Zhang, Y. Kasahara, F. Iga, W. A. Coniglio, Y. Matsuda, J. Singleton, and L. Li, Hall Anomaly, Quantum oscillations and Possible Lifshitz Transitions in Kondo Insulator YbB₁₂: Evidence for Unconventional Charge Transport, *Phys. Rev. X* **12**, 021050 (2022).
 - [18] J. Knolle and N. R. Copper, Quantum Oscillations Without a Fermi Surface and the Anomalous de Haas-Alphen Effect, *Phys. Rev. Lett.* **115**, 146401 (2015).
 - [19] L. Zhang, X.-Y. Song, and F. Wang, Quantum Oscillation in Narrow-Gap Topological Insulators, *Phys. Rev. Lett.* **116**, 046404 (2016).

- [20] P. A. Lee, Quantum oscillations in the activated conductivity in excitonic insulators: Possible application to monolayer WTe_2 , *Phys. Rev. B* **103**, L041101 (2021).
- [21] W.-Y. He and P. A. Lee, Quantum oscillation of thermally activated conductivity in a monolayer WTe_2 -like excitonic insulator, *Phys. Rev. B* **104**, L041110 (2021).
- [22] E. Tang, M. P. A. Fisher, and P. A. Lee, Low-energy behavior of spin-liquid electron spectral functions, *Phys. Rev. B* **87**, 045119 (2013).
- [23] X.-G. Wen and P. A. Lee, Theory of Underdoped Cuprates, *Phys. Rev. Lett.* **76**, 503 (1996).
- [24] P. A. Lee, N. Nagaosa, T.-K. Ng, and X.-G. Wen, $SU(2)$ formulation for the t - J model: Application to underdoped cuprates, *Phys. Rev. B* **57**, 6003 (1998).
- [25] S. Qiao, X. Li, N. Wang, W. Ruan, C. Ye, P. Cai, Z. Hao, H. Yao, X. Chen, J. Wu, Y. Wang, and Z. Liu, Mottness Collapse in $1\text{T-TaS}_{2-x}\text{Se}_x$ Transition-Metal Dichalcogenide: An Interplay Between Localized and Itinerant Orbitals, *Phys. Rev. X* **7**, 041054 (2017).
- [26] C. J. Butler, M. Yoshida, T. Hanaguri, and Y. Iwasa, Mottness versus unit-cell doubling as the driver of the insulating state in 1T-TaS_2 , *Nat. Commun.* **11**, 2477 (2020).
- [27] C. J. Butler, M. Yoshida, T. Hanaguri, and Y. Iwasa, Doubonlike Excitations and Their Phononic Coupling in a Mott Charge-Density-Wave System, *Phys. Rev. X* **11**, 011059 (2021).
- [28] S. Shen, C. Wen, P. Kong, J. Gao, X. Luo, W. Lu, Y.-P. Sun, G. Chen, and S. Yan, Inducing and tuning Kondo screening in a narrow-electronic-band system, *Nat. Commun.* **13**, 2156 (2022).
- [29] Y. Chen, W. Ruan, M. Wu, S. J. Tang, H. Ryu, H. Z. Tsai, R. Lee, S. Kahn, F. Liou, C. H. Jia, O. R. Albertini, H. Y. Xiong, T. Jia, Z. Liu, J. A. Sobota, A. Y. Liu, J. E. Moore, Z. X. Shen, S. G. Louie, S. K. Mo *et al.*, Strong correlations and orbital texture in single-layer 1T-TaSe_2 , *Nat. Phys.* **16**, 218 (2020).
- [30] Y. Chen, W.-Y. He, W. Ruan, J. Hwang, S. Tang, R. L. Lee, M. Wu, T. Zhu, C. Zhang, H. Ryu, F. Wang, S. G. Louie, Z.-X. Shen, S.-K. Mo, P. A. Lee, and M. F. Crommie, Evidence for a spinon Kondo effect in cobalt atoms on single-layer 1T-TaSe_2 , *Nat. Phys.* **18**, 1335 (2022).
- [31] W. Ruan, Y. Chen, S. Tang, J. Hwang, H.-Z. Tsai, R. Lee, M. Wu, H. Ryu, S. Kahn, F. Liou *et al.*, Evidence for quantum spin liquid behavior in single-layer 1T-TaSe_2 from scanning tunneling microscopy, *Nat. Phys.* **17**, 1154 (2021).
- [32] V. Vaño, M. Amini, S. C. Ganguli, G. Chen, J. L. Lado, S. Kezilebieke, and P. Liljeroth, Artificial heavy fermions in a van der Waals heterostructure, *Nature (London)* **599**, 582 (2021).
- [33] C. J. Butler, M. Yoshida, T. Hanaguri, and Y. Iwasa, Behavior under magnetic field of resonance at the edge of the upper Hubbard band in 1T-TaS_2 , *Phys. Rev. B* **107**, L161107 (2023).
- [34] L. B. Ioffe and A. I. Larkin, Gapless fermions and gauge fields in dielectrics, *Phys. Rev. B* **39**, 8988 (1989).
- [35] P. A. Lee and N. Nagaosa, Gauge theory of the normal state of high- T_c superconductors, *Phys. Rev. B* **46**, 5621 (1992).
- [36] O. I. Motrunich, Variational study of triangular spin-1/2 model with ring exchanges and spin liquid state in κ -(ET) $_2\text{Cu}_2(\text{CN})_3$, *Phys. Rev. B* **72**, 045105 (2005).
- [37] T. Senthil, Theory of a continuous Mott transition in two dimensions, *Phys. Rev. B* **78**, 045109 (2008).
- [38] T. Senthil, Critical Fermi surfaces and non-Fermi liquid metals, *Phys. Rev. B* **78**, 035103 (2008).
- [39] W.-Y. He, X. Y. Xu, G. Chen, K. T. Law, and P. A. Lee, Spinon Fermi Surface in a Cluster Mott Insulator Model on a Triangular Lattice and Possible Application to 1T-TaS_2 , *Phys. Rev. Lett.* **121**, 046401 (2018).
- [40] S. Florens and A. Georges, Slave-rotor mean-field theories of strongly correlated systems and the Mott transition in finite dimensions, *Phys. Rev. B* **70**, 035114 (2004).
- [41] See Supplemental Material at <https://link.aps.org/supplemental/10.1103/PhysRevB.107.195155> for (1) the slave rotor mean field description for the $U(1)$ QSL; (2) the derivation of the electronic Green's function in the $U(1)$ QSL; (3) the calculation of the electronic DOS of the $U(1)$ QSL in an orbital magnetic field; (4) the QSL electronic DOS calculation in the triangular lattice model; (5) the effect of gauge binding on the QSL electronic DOS; (6) the derivations of the in-gap bound state binding equations; (7) the LL spectrum of the in-gap bound states; and (8) the Landau quantization of a charged particle with a general isotropic band dispersion.
- [42] M. Hermele, T. Senthil, M. P. A. Fisher, P. A. Lee, N. Nagaosa, and X.-G. Wen, Stability of $U(1)$ spin liquids in two dimensions, *Phys. Rev. B* **70**, 214437 (2004).
- [43] S.-S. Lee, Low-energy effective theory of Fermi surface coupled with $U(1)$ gauge field in $2 + 1$ dimensions, *Phys. Rev. B* **80**, 165102 (2009).
- [44] Z. Dai, T. Senthil, and P. A. Lee, Modeling the pseudo-gap metallic state in cuprates: Quantum disordered pair density wave, *Phys. Rev. B* **101**, 064502 (2020).
- [45] P. A. Lee, Quantum spin liquid: A tale of emergence from frustration, *J. Phys.: Conf. Ser.* **529**, 012001 (2014).
- [46] W.-Y. He and P. A. Lee, Magnetic impurity as a local probe of the $U(1)$ quantum spin liquid with spinon Fermi surface, *Phys. Rev. B* **105**, 195156 (2022).
- [47] A. H. Castro Neto, F. Guinea, N. M. R. Peres, K. S. Novoselov, and A. K. Geim, The electronic properties of graphene, *Rev. Mod. Phys.* **81**, 109 (2009).
- [48] H. Bruus and K. Flensberg, *Many-Body Quantum Theory in Condensed Matter Physics* (Oxford University Press Inc., New York, 2004).
- [49] W.-Y. He and P. A. Lee, Electronic density of states of a $U(1)$ quantum spin liquid with spinon Fermi surface. II. Zeeman magnetic field effects, *Phys. Rev. B* **107**, 195156 (2023).
- [50] A. Ghiotto, E.-M. Shih, G. S. S. G. Pereira, D. A. Rhodes, B. Kim, J. Zang, A. J. Millis, K. Watanabe, T. Taniguchi, J. C. Hone, L. Wang, C. R. Dean, and A. N. Pasupathy, Quantum criticality in twisted transition metal dichalcogenides, *Nature (London)* **597**, 345 (2021).
- [51] T. Li, S. Jiang, L. Li, Y. Zhang, K. Kang, J. Zhu, K. Watanabe, T. Taniguchi, D. Chowdhury, L. Fu, J. Shan, and K. F. Mak, Continuous Mott transition in semiconductor moiré superlattices, *Nature (London)* **597**, 350 (2021).
- [52] Y. Nakata, K. Sugawara, R. Shimizu, Y. Okada, P. Han, T. Hitosugi, K. Ueno, Takafumi Sato, and T. Takahashi, Monolayer 1T-NbSe_2 as a Mott insulator, *NPG Asia Mater.* **8**, e321 (2016).
- [53] M. Liu, J. Leveillee, S. Lu, J. Yu, H. Kim, C. Tian, Y. Shi, K. Lai, C. Zhang, F. Giustino, and C.-K. Shih, Monolayer

- 1T-NbSe₂ as a 2D-correlated magnetic insulator, *Sci. Adv.* **7**, eabi6339 (2021).
- [54] L. Liu, H. Yang, Y. Huang, X. Song, Q. Zhang, Z. Huang, Y. Hou, Y. Chen, Z. Xu, T. Zhang, X. Wu, J. Sun, Y. Huang, F. Zheng, X. Li, Y. Yao, H.-J. Gao, and Y. Wang, Direct identification of Mott Hubbard band pattern beyond charge density wave superlattice in monolayer 1T-NbSe₂, *Nat. Commun.* **12**, 1978 (2021).
- [55] Z.-Y. Liu, S. Qiao, B. Huang, Q.-Y. Tang, Z.-H. Ling, W.-H. Zhang, H.-N. Xia, X. Liao, H. Shi, W.-H. Mao, G.-L. Zhu, J.-T. Lu, and Y.-S. Fu, Charge transfer gap tuning via structural distortion in monolayer 1T-NbSe₂, *Nano Lett.* **21**, 7005 (2021).